Molecular Systems Biology 4; Article number 156; doi:10.1038/msb4100191
Citation: ***Molecular Systems Biology*** **4:156**

www.molecularsystemsbiology.com

molecular systems biology

Modeling the electron transport chain of purple non-sulfur bacteria

Steffen Klamt[1,*], Hartmut Grammel[1], Ronny Straube[1], Robin Ghosh[2] and Ernst Dieter Gilles[1]

[1] Max Planck Institute for Dynamics of Complex Technical Systems, Magdeburg, Germany and [2] Institute of Biology, University of Stuttgart, Stuttgart, Germany
* Corresponding author. Max Planck Institute for Dynamics of Complex Technical Systems, Sandtorstrasse 1, Magdeburg D-39106, Germany.
Tel.: +49 391 6110480; Fax: +49 391 6110509;
E-mail: klamt@mpi-magdeburg.mpg.de

Received 6.8.07; accepted 18.10.07

Purple non-sulfur bacteria (Rhodospirillaceae) have been extensively employed for studying principles of photosynthetic and respiratory electron transport phosphorylation and for investigating the regulation of gene expression in response to redox signals. Here, we use mathematical modeling to evaluate the steady-state behavior of the electron transport chain (ETC) in these bacteria under different environmental conditions. Elementary-modes analysis of a stoichiometric ETC model reveals nine operational modes. Most of them represent well-known functional states, however, two modes constitute reverse electron flow under respiratory conditions, which has been barely considered so far. We further present and analyze a kinetic model of the ETC in which rate laws of electron transfer steps are based on redox potential differences. Our model reproduces well-known phenomena of respiratory and photosynthetic operation of the ETC and also provides non-intuitive predictions. As one key result, model simulations demonstrate a stronger reduction of ubiquinone when switching from high-light to low-light conditions. This result is parameter insensitive and supports the hypothesis that the redox state of ubiquinone is a suitable signal for controlling photosynthetic gene expression.
Molecular Systems Biology 15 January 2008; doi:10.1038/msb4100191
Subject Categories: cellular metabolism; metabolic and regulatory networks
Keywords: photosynthesis; redox regulation; *Rhodobacter sphaeroides*; *Rhodospirillum rubrum*; ubiquinone pool

Introduction

Our current understanding of some of the most fundamental processes of life, such as the photosynthetic generation of cellular energy or the metabolic fixation of carbon dioxide and nitrogen, has been driven largely by investigating a unique group of facultative photosynthetic bacterial organisms, the purple non-sulfur bacteria (Rhodospirillaceae). The first purple bacterial reaction center (RC) was crystallized in 1985 from *Rhodopseudomonas viridis* (Deisenhofer *et al*, 1985), and high-resolution crystal structures of the light-harvesting complexes (LHCs) LH2 from *Rhodopseudomonas acidophila* (McDermott *et al*, 1995) and LH1 from *Rhodospirillum rubrum* (Karrasch *et al*, 1995) followed, thus providing a structural basis for the understanding of the photochemical reactions taking place in the photosynthetic apparatus. Furthermore, purple non-sulfur bacteria exhibit a remarkable metabolic versatility (Tabita, 1995) that, in recent years, has put a focus of research on studying regulatory mechanisms that govern gene expression in response to varying redox conditions of the environment (Bauer *et al*, 2003). Purple non-sulfur bacteria constitute an excellent model system for this purpose due to the presence of intracytoplasmic membranes (ICMs), harboring the photosynthetic RC and LHCs, which are produced depending on the environmental factors such as oxygen, light and growth substrates. The formation of ICM can easily be measured *in vivo* and provides a phenotypic marker for the activation of photosynthetic genes. For several species, complete genome sequences are now available (http://genome.jgi-psf.org/mic_home.html) and molecular methodologies for constructing mutants have been developed. During the past years, some conserved regulatory systems involved in the control of ICM expression have been identified, including the global and highly conserved RegA/RegB (PrrA/PrrB) two-component signal transduction system (Elsen *et al*, 2004), the PpsR (CrtJ) repressor (Elsen *et al*, 2005; Kovacs *et al*, 2005) and the Fnr-like transcriptional regulator FnrL (Zeilstra-Ryalls *et al*, 1997; Zeilstra-Ryalls and Kaplan, 1998). However, particularly for light regulation of ICM synthesis, the molecular signals that are involved in the initiation of signal transduction

pathways leading to photosynthetic gene expression are poorly characterized or even still unidentified. In a remarkable forward looking perspective, Cohen-Bazire *et al* (1957), who systematically investigated the overall effect of O_2 and light on synthesis of bacteriochlorophyll (BChl) and carotenoids in *Rhodobacter sphaeroides* and *R. rubrum*, concluded that the oxidation–reduction (redox) state of one component or several components of the electron transfer systems of photosynthesis and respiration functions as a cellular signal for the activation of photosynthetic genes. Despite the fact that at that time the composition of the electron transfer chains was unknown and the assumptions about basic photochemical events were wrong, their concept of redox signaling constituted a major guideline for the following biochemical and molecular biological analysis of regulatory mechanisms that control ICM synthesis in Rhodospirillaceae. This endeavor has been challenging until today. Recently, it has been hypothesized that the redox state of the membranous ubiquinone pool could play a major role in the transcriptional control of gene expression (Oh and Kaplan, 2001; Swem *et al*, 2006). However, direct experimental evidence in the form of a signal–response curve is lacking up to now, and quantitative data obtained *in vivo* of the responses of cellular redox states are scarce. Thus, despite the details now available about the molecular structures and mechanisms involved in these processes, we are still far from having a comprehensive and quantitative insight into the overall process. The estimation of how the redox states of the different components of the photosynthetic and respiratory electron transport systems will respond to a changing redox environment, for example, the availability of electron acceptors or light, is very hard to achieve by pure intuition and also difficult to determine experimentally. Therefore, mathematical modeling is an important tool for obtaining a more holistic understanding of redox metabolism and redox-mediated control of gene expression in these organisms.

In this work, we present a model of the electron transport chain (ETC) in purple bacteria that describes the qualitative effects of different redox conditions on the redox states of electron transfer components. Even though most conclusions drawn from the model simulations should be relevant for many representatives of the Rhodospirillaceae, specific parts of the model are tailored to *R. rubrum* for the following reasons: (i) The individual components of the ETC are sufficiently characterized and a large amount of physiological data are available from earlier studies (including NADH/NAD and ATP/ADP ratios provided by the work of Schön, 1969, 1971). (ii) The ratio of RCs and LH1 expression is fixed due to activation of *puf* and *puh* operons coding for the RC and LH1 polypeptides. Since *R. rubrum* does not possess LH2, no additional interfering regulatory circuits have to be considered in the model. (iii) With the development of a special growth medium for *R. rubrum* (M2SF medium) containing the two carbon sources succinate and fructose, Ghosh *et al* (1994) provided a valuable experimental tool for addressing aspects of redox signaling. Compared to a standard medium (with succinate only), growth of *R. rubrum* with the M2SF medium results in drastically increased levels of photosynthetic membranes (PM) under semi-aerobic conditions *in the dark*, which so far were only obtainable under anaerobic low-light conditions. Here, we verify our previous hypothesis, that the effect of M2SF medium could be equivalent to redox signaling under low-light conditions, particularly at the level of the ubiquinone redox state (Grammel *et al*, 2003).

As stated above, although the model considered here is tailored to *R. rubrum*, most of the results are valid also for other representatives such as *Rb. capsulatus* and *Rb. sphaeroides* and it should be easy to adapt the model to address specific questions. The composition of the ETC in these organisms is homologous, with only minor differences in the nature of the quinone and cytochrome species.

We start the model-building procedure by compiling a list of relevant components and processes yielding first a stoichiometric model of the ETC. As we will show, even such a relatively simple model enables to identify all potential operational modes of the ETC. We will then incorporate kinetic terms to describe driving forces and reaction rates as well as—in a more coarse-grained manner—regulatory events. The primary goal of this kinetic model is to deliver robust qualitative predictions on the steady-state operation of the ETC and on how the redox states of ETC components behave under different environmental conditions.

Kinetic ETC models have already been constructed and analyzed previously, for example, for the respiratory electron transport phosphorylation in mitochondria (Korzeniewski, 1996a, b; Korzeniewski and Mazat, 1996; Beard, 2005) and for photosynthesis in higher plants and algae (Berry and Rumberg, 2000). However, although respiration in mitochondria and photosynthesis in plants share some similarities with the ETC in purple bacteria, these models cannot directly be used for our purpose. More recently, Geyer and Helms (2006) and Geyer *et al* (2007) have proposed kinetic models for photosynthesis in *Rb. sphaeroides*, which were helpful, for example, in deriving stoichiometric relationships between ETC components. However, respiration and the coupling of the ETC with the central metabolism were not considered; hence, these models cannot be employed for simulating redox states of ETC components under varying growth conditions—a major objective of this work.

Results

Stoichiometric model of the ETC

Components and processes

Anoxygenic photosynthesis (under anaerobic conditions in the light) and respiration (under aerobic conditions) are the two major strategies of the Rhodospirillaceae for generating energy in the form of ATP. For both the metabolic regimens, the key processes take place in the membranous ETC, which couples the transfer of electrons, driven by redox potential differences to the generation of proton-motive force (Δp), thus catalyzing the synthesis of ATP. Figure 1 shows a scheme of the processes and components involved neglecting, for the sake of simplicity, that the Rhodospirillaceae possess actually two structurally and functionally different types of membranes. The cytoplasmic membrane (CM), harboring the components of the respiratory chain, and the ICMs, which can be isolated as chromatophores (Drews and Golecki, 1995) with the photosynthetic RCs and the LHCs. While some electron transfer

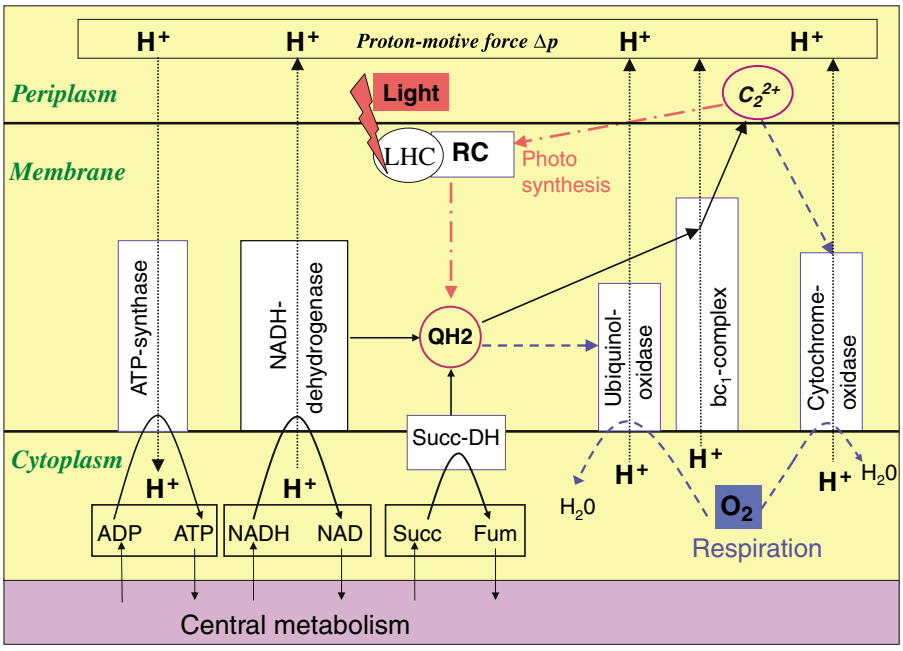

Figure 1 Main processes in the electron transport chain in purple non-sulfur bacteria. Except for proton pumping (dotted lines), all arrows inside the membrane indicate electron flows. Purely photosynthetic and purely respiratory electron flows are indicated by red dashed-dotted and blue dashed lines, respectively. Stoichiometries are not included.

components such as NADH dehydrogenase, succinate dehydrogenase, cytochrome bc_1, ATP synthase and ubiquinone are constituents of both types of membranes, others such as RC, LHC and cytochrome oxidases appear to be exclusively located in either the photosynthetic ICM or respiratory CM, respectively. Thus, CM catalyzes respiratory phosphorylation whereas ICM exclusively catalyzes photophosphorylation. Since the precise topological nature and stoichiometric composition of the two membrane compartments and their functional interactions are not yet elucidated in sufficient quantitative detail, we will not distinguish between the two types of membranes in our model, and consider instead one (combined) membrane pool. Accordingly, we also model the periplasmic space as one homogenous compartment. These assumptions simplify considerably the complicated real situation, however, as we will focus in this study on purely respiratory or purely photosynthetic growth where the main activity of the ETC is located either exclusively in the CM (respiration) or exclusively in the ICM (photosynthesis) we argue that a compartmentalized model would not change the main results of this study. In the model, the membrane will function either as a respiratory ETC or as a photosynthetic ETC and functional interactions between respiration and photosynthesis cannot take place. The different stoichiometry of CM and ICM (in particular regarding the photosynthetic apparatus) is considered in the model by incorporating regulatory pathways governing the expression of membrane components.

In the following, we compile a list of redox carriers and enzyme complexes of the ETC considered in our model (Figure 1).

Diffusible redox carriers in the membrane are *ubiquinone* (Q) and *cytochrome* c_2 (c_2). While Q is localized in the membrane, c_2 is diffusible at the P side of the membrane close to the periplasmic space. Alternative quinones (rhodoquinone in *R. rubrum*; Imhoff and Bias-Imhoff, 1995) with a more negative standard redox potential than ubiquinone are known. However, since the role of these players is not completely understood, we will not consider them herein. Also, cytochromes other than c_2 are known (Vermeglio *et al*, 1995; Zannoni, 1995), which seem to be involved mainly in respiration. Here, we will consider only one (combined) cytochrome *c* pool whose representative will be c_2.

NADH is a universal cytoplasmic carrier of reducing equivalents. In our model, NADH will represent a 'boundary' metabolite: it couples the membranous ETC with the 'rest' of the central (redox) metabolism, either by feeding electrons into the ETC or by taking up electrons from the ETC.

The *NADH-Dehydrogenase* (*NADH-DH*) couples the transfer of two electrons from NADH to Q (yielding ubiquinol, QH_2) to the translocation of cytoplasmic protons H_i^+ into the periplasm (H_p^+; here, we assume a stoichiometry of four pumped protons). The net stoichiometry of the NADH-DH thus reads:

$$\mathrm{NADH} + \mathrm{Q} + 5\mathrm{H}_i^+ \leftrightarrow \mathrm{QH}_2 + 4\mathrm{H}_p^+ + \mathrm{NAD}^+ \qquad (1)$$

Under certain circumstances, the NADH-DH can also run in the reverse direction. Purple bacteria make use of this reverse electron flow particularly under phototrophic conditions.

The *succinate dehydrogenase* (*Succ-DH*) oxidizes succinate to fumarate and passes the two electrons to ubiquinone. Protons are not pumped in this process.

$$\mathrm{Succinate} + \mathrm{Q} \leftrightarrow \mathrm{Fumarate} + \mathrm{QH}_2 \qquad (2)$$

Succ-DH is a key enzyme of the citric acid cycle, and couples the central carbon metabolism to the ETC at the level of Q. Reaction (2) may also run in the reverse direction, depending

on the concentrations of the compounds involved. Succ-DH functions then as a fumarate reductase. Alternative fumarate reductases, which are differentially expressed during anaerobic respiration with fumarate as electron acceptor, will not be considered here as additional components. Other enzyme complexes that are able to oxidize metabolites and to feed electrons into the ETC (such as glycerol dehydrogenase) are also not taken into account as they can be assumed to be of low relevance for the environmental scenarios considered herein.

The *cytochrome* bc_1 *complex* (bc_1) transfers electrons from the ubiquinol pool to cytochrome c_2 and pumps protons via a mechanism known as the Q cycle (Trumpower, 1990). The net balance of this complicated cycle reads:

$$QH_2 + 2H_i^+ + 2\,c_2^{3+} \leftrightarrow 2\,c_2^{2+} + Q + 4H_p^+ \qquad (3)$$

Whereas NADH-DH, Succ-DH and bc_1 are operative under photosynthetic as well as respiratory growth conditions (and are contained in both types of membranes), the following two oxidases are only active under aerobiosis since they mediate the irreversible transfer of electrons to the terminal acceptor oxygen (other acceptors such as DMSO can be utilized but are not relevant herein).

The *cytochrome c oxidase* oxidizes two c_2 and passes the electrons to oxygen, thereby pumping protons into the periplasm:

$$0.5\,O_2 + 2\,c_2^{2+} + 4\,H_i^+ \rightarrow 2\,c_2^{3+} + H_2O + 2H_p^+. \qquad (4)$$

Two major cytochrome *c* oxidases are known in purple bacteria. The cbb_3 oxidase having a high affinity to oxygen, and an aa_3 oxidase with a lower affinity (Zannoni, 1995). Cytochrome oxidases of the cbb_3 type are found, for example, in *Rb. sphaeroides*, *Rb. capsulatus* and *R. rubrum* (the latter based on gene sequence data, not shown), whereas from these three representatives only *Rb. sphaeroides* has been shown to possess the aa_3-type enzyme. Therefore, we will consider only the cbb_3 oxidase.

The *ubiquinol oxidase* (containing a *b*-type heme; Varela and Ramirez, 1990) transfers electrons directly from QH_2 to oxygen:

$$0.5\,O_2 + QH_2 + 2\,H_i^+ \rightarrow Q + H_2O + 2H_p^+ \qquad (5)$$

The ubiquinol oxidase functions also as a proton pump but the overall H_p^+/e^- stoichiometry is lower than using bc_1 and cytochrome oxidase. Presumably for this reason, ubiquinol oxidase is mainly expressed under semi-aerobic conditions (Swem and Bauer, 2002) where it helps to avoid an over-reduction of the ubiquinone pool.

The *photosynthetic apparatus* consists of RC and LHC (see above and Materials and methods section). Photons (ν) are harvested in the LHC and then funneled as excitations to the RC where charge separations take place leading to the reduction of Q and oxidation of c_2:

$$2\nu + Q + 2\,c_2^{2+} + 2\,H_i^+ \rightarrow QH_2 + 2\,c_2^{3+} \qquad (6)$$

Protons are not pumped during this process. The merit of the photosynthetic apparatus is the light-induced uphill (from high to low redox potential) transfer of electrons from c_2 to QH_2.

Finally, the *ATP synthase* complex converts generated Δp to chemical energy in the form of ATP. Assuming a H_p^+/P ratio of 3, the stoichiometry reads:

$$ADP^{3-} + P_i^{2-} + 3H_p^+ + H_i^+ \rightarrow ATP^{4-} + H_2O + 3H_i^+ \qquad (7)$$

Operational modes of the ETC

So far we have collected the main components and the net stoichiometries of the electron transfer processes in the ETC of purple non-sulfur bacteria. This does not yet say much about how the different processes have to be combined in a way that the ETC can bring about a coherent function. The seven stoichiometric reactions (1–7) give rise to a stoichiometric reaction network that can be described formally by a stoichiometric matrix **N** (rows: species; columns: reactions; N_{ij}= stoichiometric coefficient of species *i* in reaction *j*). We can then apply well-established tools from metabolic network analysis to understand how the ETC can operate in the steady state (Price *et al*, 2004; Klamt and Stelling, 2006). A suitable approach from this methodology is the formalism of *elementary modes* (EMs) that enables to identify operational modes (Schuster *et al*, 2000; Klamt and Stelling, 2006). EMs are defined as minimal subnetworks that can perform a function in the steady state. They correspond typically to pathways or cycles in the reaction network. Each EM is characterized by the participating reactions (and the relative fluxes they carry) and no subset of the reactions involved of an EM can sustain a steady-state flux distribution. Importantly, any potential steady-state behavior of a metabolic network can be described as a non-negative superposition of the EMs.

Since the ETC is a subsystem of the whole system 'cell', applying the approach of EMs requires the definition of model boundaries. In our case, we have to specify which compounds are coupled to other processes taking place outside the ETC. This concerns (from here, we omit molecule charges) NAD, NADH, ADP, ATP, succinate, fumarate, photons, P_i, H_i, H_2O and O_2 which are considered to be *external* metabolites (Klamt and Stelling, 2006). For these metabolites, we do not demand a steady-state (mass balance) condition since they can be produced, consumed, exported or imported elsewhere in the metabolism. In contrast, reduced and oxidized forms of ubiquinone and cytochrome c_2 as well as the protons in the periplasm (H_p) are considered as *internal* metabolites, that is they have to be kept in a balanced state. Accordingly, the stoichiometric matrix **N** for the internal species of the ETC reads (the seven columns (reactions) correspond to the equations (1–7)):

$$\mathbf{N} = \begin{pmatrix} 1 & 1 & -1 & 0 & -1 & 1 & 0 \\ -1 & -1 & 1 & 0 & 1 & -1 & 0 \\ 0 & 0 & 2 & -2 & 0 & -2 & 0 \\ 0 & 0 & -2 & 2 & 0 & 2 & 0 \\ 4 & 0 & 4 & 2 & 2 & 0 & -3 \end{pmatrix} \begin{matrix} \rightarrow QH2 \\ \rightarrow Q \\ \rightarrow c_2^{2+} \\ \rightarrow c_2^{3+} \\ \rightarrow H_p^+ \end{matrix}$$

For this stoichiometric configuration of the ETC, in total, nine EMs can be computed (e.g. with *CellNetAnalyzer*; Klamt *et al*, 2007). The stoichiometry of these modes is summarized in Table I, a schematic representation is given in Figure 2. The EMs have been ordered with respect to the Δp-generating process, namely photosynthesis (EM1 and EM2), oxidative respiration (EM3–EM8) and fumarate reduction (EM9). Most EMs correspond to well-known functions of the ETC in purple

Table I Elementary modes in the electron transport chain of purple non-sulfur bacteria

Overall stoichiometries of the reactions in the ETC	Photosynthesis	Respiration					Fumarate reduction
	ATP synthesis	Reverse electron flow		ATP synthesis			
	EM1	EM2	EM3	EM4	EM5	EM6	EM7	EM8	EM9
NADH-DH: $NADH \leftrightarrow 4H_p + QH_2$		−1	−1	−3			2	6	3
Succ-DH: $succinate \leftrightarrow QH_2$		1	3	5	6	2			−3
bc_1: $QH_2 \leftrightarrow 2c_2 + 4H_p$	3	1		2		2		6	
c-Oxidase: $2c_2 + 0.5O_2 \rightarrow 2H_p$				2		2		6	
Q-Oxidase: $QH_2 + 0.5O_2 \rightarrow 2H_p$			2		6		2		
RC: $2c_2 + 2\nu \rightarrow QH_2$	3	1							
ATP synthase: $3H_p \rightarrow ATP$	4				4	4	4	20	4
Balance of external metabolites									
ν (photons)	−6	−2							
NADH (negative to NAD)		+1	+1	+3			−2	−6	−3
Succinate (negative to fumarate)		−1	−3	−5	−6	−2			3
O_2			−1	−1	−3	−1	−1	−3	
ATP (negative to ADP)	+4				+4	+4	+4	+20	4

To be concise and without changing the results, ADP, NAD, P_i, cytoplasmic protons (H_i^+), H_2O, the oxidized forms of each redox pair (Q, c_2^{3+}, fumarate) as well as the molecule charges were omitted in the reaction equations. The pools of ubiquinone, cytochrome c_2 and protons in the periplasm (H_p) were considered as internal (balanced) metabolites and all others as external (the overall stoichiometry for some external metabolites is shown for each EM; for internal metabolites, the overall stoichiometry is zero in each EM by definition). All numerical values represent flux values in arbitrary units (e.g. mmol/gDW h). See also Figure 2.

bacteria. The photosynthetic lifestyle can be described by just two EMs: EM1 is the cyclic photophosphorylation that produces ATP at the expense of absorbed photons by cycling electrons from ubiquinol to cytochrome c_2 (via bc_1) and back to ubiquinol (via the RC). EM1 reproduces correctly the fact that the cyclic photophosphorylation does not consume electrons in the overall stoichiometry. EM2 reflects another important function of the ETC under photosynthetic conditions, namely reverse electron flow: Δp is generated via photosynthesis and then utilized for an active transfer of electrons from succinate via QH_2 to NADH. This process is essential for growth on substrates such as succinate or propionate whose electrons enter the ETC at the level of QH_2 via Succ-DH. These electrons have to be withdrawn from the ETC because under anaerobic growth no electron consuming processes take place in the ETC (at least not in the processes considered in our model) and an accumulation of electrons and thus over-reduction of the ETC would follow.

Reverse electron flow is rarely considered for respiratory growth, although two EMs reflect that this is stoichiometrically feasible: the energy (Δp) required for the uphill transport of electrons from succinate to NADH is generated via ubiquinol oxidase (EM3) or cytochrome oxidase (EM4). Most likely, these operational modes play only a minor role under fully aerobic conditions since the ETC is then in an oxidized state and electrons will be strongly attracted by oxygen due to its high redox potential. However, reverse electron flow under respiratory conditions may occur as an important (short-term) phenomenon under situations where a strong imbalance in the redox potentials of NADH/NAD (concentration ratio low) and succinate/fumarate (concentration ratio high) occurs: electrons may flow with 'high pressure' from succinate into the ETC and proton-motive force generated by respiration may then partially be used to drain electrons from the ETC for reducing NAD.

EM5–EM8 describe the four different ways of ATP synthesis during respiration. Two possible electron suppliers (NADH and succinate) and two available oxidases (ubiquinol oxidase and cytochrome oxidase) give rise to these four EMs. The optimal ATP yield is achieved with NADH as electron donor and cytochrome oxidase (EM8), the lowest yield, as expected, results with succinate and ubiquinol oxidase (EM5). As mentioned above, ubiquinol oxidase is mainly expressed under semi-aerobic conditions where the lower ATP yield is counterbalanced by the effect of draining electrons out of the ETC, thus preventing over-reduction.

The last EM (EM9) represents fumarate reduction, another well-known operation of the ETC enabling ATP synthesis by anaerobic respiration if neither light nor oxygen is available (Zannoni, 1995).

We have not considered proton leak in the stoichiometric model, but we note that all EMs that produce ATP (EM1, EM5–EM9) could alternatively be used for compensating uncoupled efflux of protons from peri- to cytoplasm.

As already mentioned, the actual flux pattern in the ETC is usually a superposition of EMs (see Figure 4 discussed in a later section). For example, under photosynthetic conditions, cyclic photosynthesis (EM1) and reverse electron flow (EM2) do usually operate concurrently. Respiratory and photosynthetic EMs may be combined when the bacteria are exposed to light and oxygen.

EM analysis thus provides useful insights into the basic functional and operational modes of the ETC. However, these are potential modes and to predict the activity of these modes for a particular situation, the concentrations and redox states of components must be considered explicitly. For example, the amount of Δp and the redox states of NADH and the ubiquinone pool determine whether forward or reverse electron flow takes place at the NADH-DH. Furthermore, for understanding why redox states in the ETC may serve as regulatory signals for controlling gene expression, we require a dynamic description based on differential equations.

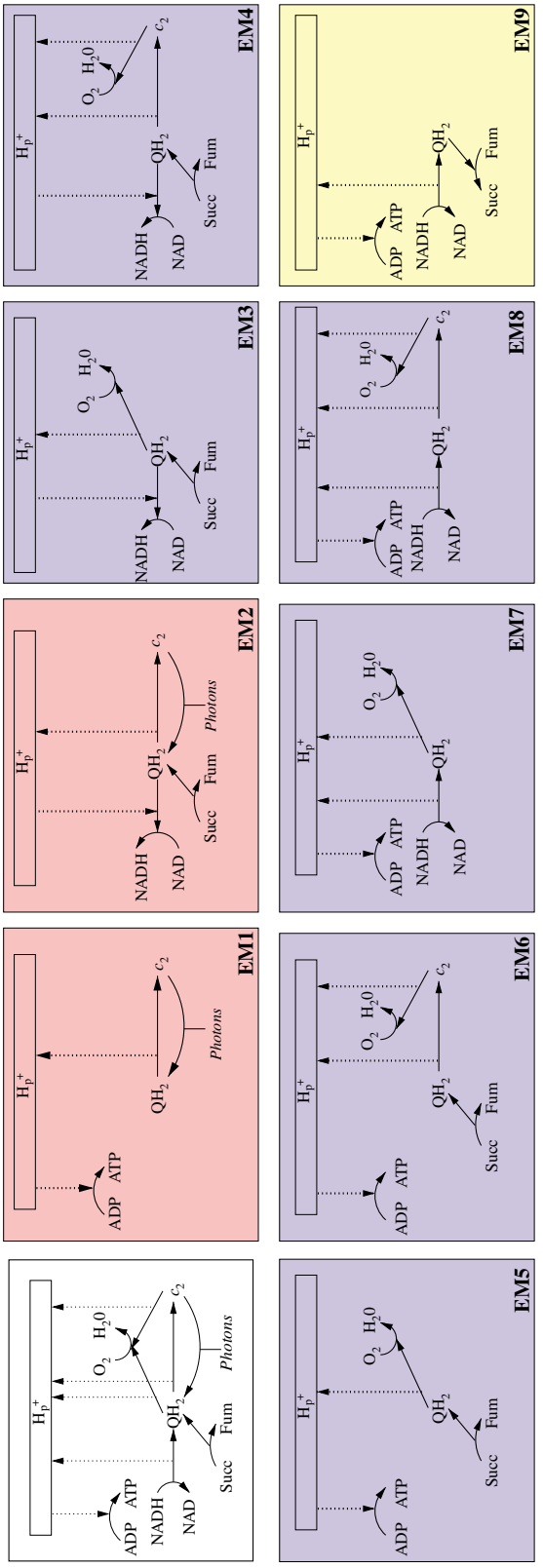

Figure 2 The fundamental operational modes (elementary modes) of the electron transport chain in purple non-sulfur bacteria. Stoichiometries (i.e. relative reaction rates) have been omitted and can be seen in Table I. In the upper left corner, the full network is depicted (compressed version of Figure 1).

Kinetic model of the ETC

The kinetic model—described in detail in the Materials and methods section and in Tables III and IV—comprises the electron transfer processes of the ETC as depicted in Figure 1. The key question in the development of the ETC model was how to describe kinetically the complicated electron transfer processes. Here, we followed the approach of Korzeniewski (1996a, b) and Korzeniewski and Mazat (1996) by modeling the entirety of elementary steps taking place at an enzyme complex as one (overall) redox reaction. The overall stoichiometries of these redox reactions correspond to the equations (1–6) and their driving forces are redox potential differences between the redox couples involved (see Materials and methods). Korzeniewski and co-workers modeled the respiratory chain of mitochondria that exhibits some homologies to the ETC of Rhodospirillaceae, though the latter possesses additionally the photosynthetic phosphorylation cycle.

For quantifying redox potentials (and redox potential differences), one requires the concentration ratios of the reduced/oxidized forms of the relevant redox couples, namely $[QH_2]/[Q]$, $[c_2^{2+}]/[c_2^{3+}]$, [NADH]/[NAD] and [succinate]/[fumarate] (see Materials and methods). Whereas [Q], $[QH_2]$ $[c_2^{3+}]$ and $[c_2^{2+}]$ are state variables in the model, we cannot proceed in the same way with [NADH], [NAD], [succinate] and [fumarate] as these compounds are involved in many other metabolic reactions taking place outside the ETC. Here, we face a general problem in modeling cellular processes: how to delimit the modeled processes from the rest of the cell? We employ the following strategy: for each of the growth regimens considered—for example, aerobic growth in the dark or anaerobic growth in light—we clamp the concentration ratios of external metabolites such as [NADH]/[NAD] to a specific value (obtained from measurement data). The advantage is that we do not need to model the whole cell to get a complete balance for these compounds. However, in a simulation, the assumed (steady state) ratio is immediately fixed after changing the environmental conditions. For this reason, we will focus herein on the steady-state behavior of the kinetic model (which is nevertheless fundamentally different to the approach of EMs since steady-state concentrations of metabolites are explicit state variables.). There are also other reasons why our model allows only for steady-state analysis. As we consider only overall reactions inside the protein complexes, any reaction is immediate and does not reflect the time course of events inside the protein that may lead to wrong simulation results for the very early response of the ETC. Moreover, the buffer capacity (captured by the parameter *piV*; see Materials and methods section), which determines how fast the ETC can adapt after changing metabolite concentrations, is insensitive against the steady-state data used to fit the experiments (see below) and thus badly determined.

Though the main application of our kinetic model is to simulate the steady-state operation of the ETC under different environmental conditions, we need to include basic regulatory events such that the photosynthetic apparatus consisting of LHC and RC is synthesized under anaerobic conditions. As already mentioned above, the composition of the ETC and the formation of photosynthetic membranes in purple bacteria are mainly governed by the external signals oxygen and, to a lower extent, light intensity and the supply of reducing equivalents by the carbon substrate. Three major regulators (RegB/RegA (PrrB/PrrA), FnrL and PpsR (CrtJ)) have been identified that control the expression of genes involved in the synthesis of the photosynthetic gene cluster (PGC; Alberti *et al*, 1995) and other ETC components such as ubiquinone, c_2 as well as of the ubiquinol and the cytochrome (cbb_3) oxidase (see Oh and Kaplan, 2001; Bauer, 2004 and Materials and methods). In a coarse-grained manner, we included kinetic terms in the differential equations for LHC, RC and other ETC components that account for the combined effects of the three regulators (see Materials and methods).

Interestingly, none of the above-mentioned regulators is able to sense light directly. Instead it has been suggested that different light intensities are indirectly measured via the redox state of the ubiquinone pool (Swem *et al*, 2006). In fact, we want to examine whether our model supports this hypothesis.

In total, the model comprises 33 time-dependent variables of which 10 are states (expressed by ordinary differential equations); the rest depends algebraically upon the state variables (Table III). The model has 55 parameters (Table IV); 17 of them could be directly taken from literature values. The other parameters were estimated by fitting the measurement data—taken from different growth scenarios—as given in Table II. We implemented and simulated the ETC model with self-written MATLAB scripts and implemented it additionally with the Systems Biology Toolbox (Schmidt and Jirstrand, 2006; http://www.sbtoolbox.org/) for MATLAB. The model file for the Systems Biology Toolbox can be downloaded from http://www.mpi-magdeburg.mpg.de/projects/cna/etcmodel.html.

Model analysis and simulations

In the simulations, we focused on four different environmental regimens (Table II): aerobic (R1) and semi-aerobic (R2) in dark conditions; anaerobic under high-light (R3) and low-light (R4) conditions. The four growth regimens are thus characterized by the imposed oxygen tension and mean irradiance, for which we have chosen typical values reported in the literature.

As explained above, for each simulation, the three concentration ratios [NADH]/[NAD], [succinate]/[fumarate] and [ATP]/[ADP] have to be clamped (but can be varied in different simulations). We abbreviate these ratios in the following with $\mathbf{R}_{NADH}$, $\mathbf{R}_{Succ}$ and $\mathbf{R}_{ATP}$, respectively. The respective ratios chosen for the four different growth regimens are also shown in Table II. Regarding $\mathbf{R}_{Succ}$, we assumed unity since no appropriate measurements could be found in the literature. For $\mathbf{R}_{ATP}$, some values are available in Schön (1969) showing comparable values for aerobic and photosynthetic growth of *R. rubrum* on succinate. We therefore opted to use an average value of 2.7 for all conditions. Regarding the ratio of $\mathbf{R}_{NADH}$, Schön (1971) presented data for three of the four different growth regimens; an estimate was made for low-light growth (R4). In addition to $\mathbf{R}_{NADH}$, $\mathbf{R}_{Succ}$ and $\mathbf{R}_{ATP}$, we found a number of measurements of ETC components in the literature, which have been used for parameter fitting (see Table II and Figure 3, where the circles indicate a sufficiently good fitting result).

Table II Four growth regimens simulated with the ETC model together with published measurements of model variables used for parameter fitting

	R1: aerobic growth in the dark	R2: semi-aerobic growth in the dark	R3: anaerobic growth in high light	R4: anaerobic growth in low light
Oxygen tension (%)	9.9	0.1	0	0
Mean irradiance, μE/s m^2 (W/m^2)	0	0	440 (95.6) (Holt and Marr, 1965)	7.3 (1.59) (Holt and Marr, 1965)
$\mathbf{R}_{Succ}$: [Succinate]/[Fumarate]	1[a]	1[a]	1[a]	1[a]
$\mathbf{R}_{ATP}$: [ATP]/ADP]	2.7[a] Schön (1969)	2.7[a] (Schön, 1969)	2.7[a] (Schön, 1969)	2.7[a] (Schön, 1969)
$\mathbf{R}_{NADH}$: [NADH]/[NAD] (Schön, 1971)	0.051 (Schön, 1971)	0.71 (Schön, 1971)	0.21 (Schön, 1971)	0.71[a] (Schön, 1971)
Measurements (in parentheses: name of the corresponding model variable (see Table III))				
Q_{total} (Qt)	1.31 (Carr and Exell, 1965)		2.52 (Carr and Exell, 1965)	
QH_2/Q_{total} (*Q_charge*)	0.17[b] (Zannoni, 1995)		0.53 (Redfarn, 1967)	
Bacteriochlorophyll (*Bchl*)	0.05 (Grammel *et al*, 2003)	1.22 (Grammel *et al*, 2003)	2.17 (Holt and Marr, 1965)	8.20 (Holt and Marr, 1965)
cbb$_3$-Oxidase (*Oxi_t*)	1.5[c] (Swem and Bauer, 2002)	4.5[c] (Swem and Bauer, 2002)		
Ubiquinol oxidase (*UbiOxi_t*)	0.5[c] (Swem and Bauer, 2002)	1.5[c] (Swem and Bauer, 2002)		
μ (*mue*)	0.154 (Grammel *et al*, 2003)	0.10 (Holt and Marr, 1965)	0.14 (Holt and Marr, 1965)	0.10 (Holt and Marr, 1965)

For oxygen tension and mean irradiance (sun light), typical values have been chosen (unit 'E' (Einstein) denotes 1 mol photons and 1 μE/s m^2 = 0.217 W/m^2). References for measurements are given. Measurement units are μmol/gDW (for BChl and Q_{total}), h^{-1} (for μ) and dimensionless for the others (see also Table III).
[a]Estimated values (see explanations in main text).
[b]In reference Zannoni (1995), the reduction degree of ubiquinone for aerobic conditions was estimated between 4 and 30%; here we chose the average.
[c]The values for the relative concentrations of *cbb*$_3$ and ubiquinol oxidases have been estimated from expression ratios given in Swem and Bauer (2002).

Although the chosen values for $\mathbf{R}_{NADH}$, $\mathbf{R}_{Succ}$ and $\mathbf{R}_{ATP}$ should reflect the situations for the different growth regimens, their precise value will not only depend on the imposed light intensity and oxygen concentration (as assumed in Table II) but also on other external factors such as the reduction degree and energy content of the substrate. Therefore, it makes sense to vary these ratios and to study how this affects the steady-state behavior of the ETC in the different growth regimens.

Model simulations: varying the cellular [NADH]/[NAD] ratio

$\mathbf{R}_{NADH}$ is an important measure of the overall redox state of the cell and is strongly coupled with the ETC and therefore of paramount importance for our investigations. For studying the response of the ETC to different levels of $\mathbf{R}_{NADH}$, we varied this value (in all growth regimens) within a physiologically meaningful range between 0.01 and 2.01 and computed the resulting steady states in the system. In this way, we obtained response curves of ETC components with respect to the cytoplasmic redox state (Figure 3), which will be discussed below.

Note that $\mathbf{R}_{NADH}$ will not only influence the redox state of ETC but also depends on the redox state of the ETC. However, here we consider $\mathbf{R}_{NADH}$ as an independent variable so that a certain value of $\mathbf{R}_{NADH}$—for example, measured in a particular experiment—can be directly related to the corresponding electron flows and (redox) states of components in the ETC.

Aerobic growth (regimen R1)

As expected, in the fully aerobic case we have the lowest redox charge of the ubiquinone and c_2 pool of all growth regimens (see Figure 3: *Q_charge* (QH_2/Q_{total}) and *c2_charge* ($c_2^{2+}/c_{2,total}$)). We can conclude that a low cytoplasmic redox potential, for example, generated by a strongly reduced substrate, will not limit the operation of the ETC; the opposite is the case as a higher value for $\mathbf{R}_{NADH}$ increases the electron flow. The reason is that oxygen withdraws the electrons—fed in by the NADH-DH and Succ-DH—quickly from the ETC. We also notice that the transport of electrons to oxygen is mainly catalyzed via the *cbb*$_3$ oxidase as the ubiquinol oxidase is not expressed under strong aerobic conditions (Swem and Bauer, 2002) (see Figure 3).

To relate the results of the kinetic model to the EM analysis (Table I; Figure 2), we also computed for each scenario the relative contribution of the nine EMs (Figure 4; see Materials and methods section). Regarding the aerobic regimen, we can summarize that the ETC is mainly driven by the two elementary modes EM6 and EM8 and the relative proportion of EM8 (which uses the NADH-DH) increases with $\mathbf{R}_{NADH}$ (Figure 4). Neither fumarate reduction (EM9) nor reverse electron transport (EM3 and EM4) takes place; these modes become only active if $\mathbf{R}_{NADH}$ is extremely high (and/or $\mathbf{R}_{Succ}$ extremely low) or vice versa, respectively.

If we consider *identical* $\mathbf{R}_{NADH}$ values for all four growth regimens, aerobic growth results in the highest Δp. However, this condition is not necessarily valid for the real physiological situation. Since experimental data show that $\mathbf{R}_{NADH}$ is usually low under aerobic and higher under anaerobic growth (Table II), we might nevertheless observe a higher Δp for photosynthetic conditions. Importantly, and this applies for all growth regimens, the Δp values that were computed in the

Table III State (S) and algebraic (A) variables of the electron transport chain model

Name (unit)	Type	Differential/algebraic equation	Remarks
Qt (μmol/gDW)	S	Qt′ = *Ubistoich* · c2_synth−mue · Qt	Total concentration of ubiquinone
QH2 (μmol/gDW)	S	QH2′ = 1000 · (NADH_DH_flux −bc1_flux + RC_flux + Succ_DH_flux)−mue · QH2	Concentration of reduced ubiquinone (ubiquinol)
Q (μmol/gDW)	A	Q = Qt−QH2	Free oxidized ubiquinone
Q_charge (−)	A	Q_charge = QH2/Qt	Reduction degree of ubiquinone
c2t (μmol/gDW)	S	c2t′ = c2_synth−mue · c2t	Total concentration of cytochrome c_2
c2red (μmol/gDW)	S	c2red′ = 1000 · (2 · bc1_flux−2 · Oxi_flux−2 · RC_flux)−mue · c2red	Concentration of reduced c_2
c2ox (μmol/gDW)	A	c2ox = c2t−c2red	Concentration of oxidized c_2
c2_charge (−)	A	c2_charge = c2red/c2t	Reduction degree of c_2
c2_synth (μmol/gDW h)	A	c2_synth = *K1* · ***inh***(*pO2*,*Km2*,*E2*) · ***inh***(*c2t*,*Km1*,*E1*) + *K1c* · mue	Synthesis rate of c_2 (Q and bc_1 are synthesized in a fixed ratio)
Oxi_t (−)	S	Oxi_t′ = *K3* · ***hill***(*pO2*,*Km3*,*E3*) · ***inh***(*pO2*,*Km3i*,*E3i*) + *K3c* · mue−mue · Oxi_t	(Relative) concentration of cbb_3 oxidase
Oxi_red (−)	A	Oxi_red = Oxi_t/(c2ox/c2red · ***exp***((pmf + dpsi−*Em_b3* + *Em_c2*)/*ZZ*) + 1)	(Relative) concentration of cbb_3 oxidase reduced in cytochrome b_3; assumptions: (a) b_3 is in equilibrium with c_2 (b) for each electron transferred from c_2 to b_3 one proton is pumped into the periplasmic space; see text and Korzeniewski (1996b)
Oxi_flux (mmol/gDW h)	A	Oxi_flux = *K_Ox* · Oxi_red · c2red · ***hill***(*pO2*,*Km_Oxi*,*Exp_Oxi*)	Flux through cbb_3 oxidase
UbiOxi_t (−)	S	UbiOxi_t′ = *K4c* · mue + *K4* · ***hill***(*pO2*,*Km4*,*E3*) · ***inh***(*pO2*, *Km4i*,*E3i*)−mue · UbiOxi_t	Relative concentration of ubiquinol oxidase
UbiOxi_red (−)	A	UbiOxi_red = UbiOxi_t/(Q/QH2 · ***exp***((pmf−*Em_b_UbiOxi* + *Em_Q*)/*ZZ*) + 1)	(Relative) concentration of ubiquinone oxidase reduced in *b*-type cytochrome; analogous assumptions as for Oxi_red
UbiOxi_flux (mmol/gDW h)	A	UbiOxi_flux = *K_UbiOxi* · UbiOxi_red · QH2 · ***hill***(*pO2*,*Km_UbiOxi*,*Exp_UbiOxi*)	Flux through ubiquinol oxidase
bc1 (μmol/gDW)	S	bc1′ = *bc1stoich* · c2_synth−mue · bc1	Concentration of bc_1 complexes (monomers, not dimers)
bc1_flux (mmol/gDW h)	A	bc1_flux = *K_bc1* · bc1 · (*Em_c2* + *ZZ* · ***ln***(c2ox/c2red)−(*Em_Q* + *ZZ*/2 · ***ln***(Q/QH2))−2 · pmf + dpsi)	Flux through bc_1 complex (see Materials and methods section)
LHC (μmol/gDW)	S	LHC′ = PSC_synth−mue · LHC	Light-harvesting complex (here only LH1 considered; see text)
RC (μmol/gDW)	S	RC′ = PSC_synth−mue · RC	Concentration of reaction centers
Bchl (μmol/gDW)	A	Bchl = 4 · RC + 32 · LHC	Bchl concentration (*R. rubrum*)
PSC_synth (μmol/gDW h)	A	PSC_synth = K2 · ***inh***(*pO2*,*Km2*,*E2*) · ***hill***(Q_charge,*Km2Q*,*E2Q*) · ***inh***(RC,*Km2RC*,*E2RC*)	Synthesis rate of photosynthetic complexes; with saturation term
light_harvesting (mE/gDW h)	A	light_harvesting = *K_lh* · LHC · ***hill***(*mean_irradiance*,*Km_lightint*, *Exp_lightint*)	Photon absorption rate in LHC
RC_flux (mmol/gDW h)	A	RC_flux = *K_RC* · RC · ***hill***(light_harvesting/RC,*Km_lh*,*Exp_lh*) · (c2red^2 · Q · ***exp***(−2/*ZZ* · dpsi)−QH2 · c2ox^2 · ***exp***(−2/*ZZ* · (*Em_Q*−*Em_c2* + 1340)))	
NADH_DH_flux (mmol/gDW h)	A	NADH_DH_flux = *K_NADHDH* · (*Em_Q* + *ZZ*/2 · ***ln***(Q/QH2)−(−320 + *ZZ*/2 · ***ln***(1/*Rnadh*))−pmf · 2)	Flux through NADH-DH
Succ_DH_flux (mmol/gDW h)	A	Succ_DH_flux = *K_SuccDH* · (*Em_Q* + *ZZ*/2 · ***ln***(Q/QH2)−(31 + *ZZ*/2 · ***ln***(1/*Rsucc*)))	Flux through Succ-DH
ATPSynthase_flux (mmol/gDW h)	A	ATPSynthase_flux = *K_ATPS* · (***exp***(*kk*/(*RR* · *TT*)) −1)/(***exp***(*kk*/(*RR* · *TT*)) + 1) with *kk* = (3 · pmf · *FF*−30.5−*RR* · *TT* · ***ln***(*Ratp*/*Phos*))	Flux through ATP synthase
mue (h^{-1})	A	mue = *mue_max* · ***hill***(*ATPSynthase_flux*,*Km_mue*,*Exp_mue*)	Growth rate; here: ATP-limited
Hp (mM)	S	Hp′ = *piV* · (4 · NADH_DH_flux + 4 · bc1_flux + 2 · Oxi_flux + 2 · UbiOxi_flux−3 · ATPSynthase_flux)−proton_leak−mue · Hp	Proton concentration in the periplasm
pHp (−)	A	pHp = −***log10***(Hp/1000)	pH in periplasm
DeltapH (−)	A	deltapH = *pHi*−pHp	−ΔpH
pmf (mV)	A	pmf = 1/(1−*psi_p*) · 2.303 · *ZZ* · deltapH	Δ*p* (proton-motive force)
dpsi (mV)	A	dpsi = *psi_p* * pmf	ΔΨ (membrane potential)
proton_leak (mM/h)	A	proton_leak = *K_leak* · (pmf−160)	Expression taken from Korzeniewski (1996a)

Parameters are written in italic. ***hill*** expresses standard Hill kinetics: ***hill***(S,K,c) = S^c/(S^c + K^c) and ***inh*** a standard inhibition term: ***inh***(I,K,c) = K^c/(I^c + K^c). Furthermore, *exp*(*x*) = e^x, ***ln*** is the natural and ***log10*** the decadian logarithm. gDW stands for 'gram dry weight.' Several equations are derived or explained in the Materials and methods section.

Table IV Parameters of the electron transport chain model

Symbol	Value	Remarks
mean_irradiance	see Table II	In μE/s m^2; value depends on chosen growth regimen (Table II)
pO2	see Table II	Oxygen tension (% saturation); value depends on chosen growth regimen (Table II)
Rnadh	see Table II	[NADH]/[NAD]; value depends on chosen growth regimen (Table II)
Ratp	see Table II	[ATP]/[ADP]; value depends on chosen growth regimen (Table II)
Rsucc	see Table II	[Succinate]/[Fumarate]; value depends on chosen growth regimen (Table II)
FF	0.0965 KJ/mol mV	Faraday constant
RR	0.0083 KJ/mol K	Gas constant
TT	298 K	Temperature
ZZ	25.631 mV	ZZ = RR · TT/FF
Em_Q	70 mV	Midpoint redox potential of ubiquinone
Em_c2	340 mV	Midpoint redox potential of cytochrome c_2 (Garcia *et al*, 1987)
Em_b_UbiOxi	250 mV	Midpoint redox potential of cytochrome *b* in ubiquinol oxidase (Varela and Ramirez, 1990)
Em_b3	540 mV	Midpoint redox potential of cytochrome b_3 in cbb_3 oxidase; analogous to Korzeniewski (1996b)
pHi	7	Cytosolic pH
Phos	0.001 M	Cytosolic phosphate concentration
psi_p	0.7	Relative contribution of $\Delta\Psi$ (membrane potential) to pmf (estimated from Wraight *et al* (1978): ΔpH $\approx 1 \rightarrow \Delta\Psi/\Delta p \approx 0.7$)
piV	10 mM/mmol/gDW	Expresses the change of periplasmic proton concentration (mM) if 1 mmol cytosolic protons per gDW is pumped over the membrane; this value depends on buffer capacities and volume ratios (estimated; but steady-state results are insensitive against this parameter)
mue_max	0.17 h^{-1}	Maximal growth rate (for *R. rubrum*; from own experiments; see also Grammel *et al* (2003) and Holt and Marr (1965)
Km_mue	8.5 mmol/gDW h	Half the rate of ATP synthase if the cell grows with maximal growth rate (0.17 h^{-1}); estimated from a stoichiometric model (Klamt *et al*, 2002) for photosynthetic growth on succinate (a similar value follows for respiratory growth)
Exp_mue	4	
Ubistoich	25	Approximated concentration ratio Qt/c2 (Garcia *et al*, 1987)
bc1stoich	0.6	Approximated concentration ratio bc1/c2 (Garcia *et al*, 1987)
K_ATPS	20.0 mmol/gDW h	
K_NADHDH	3.35 mmol/gDW h mV	
K_SuccDH	0.02 mmol/gDW h mV	
K_bc1	67 mmol/h mV μmol	
K_leak	0.08 mmol/h l mV	
K_Oxi	13000 mmol/h μmol	
Km_Oxi	0.55 %	
Exp_Oxi	3	
K_UbiOxi	6.5 mmol/h μmol	
Km_UbiOxi	0.2 %	
Exp_UbiOxi	3	
K_lh	500 mE/h μmol	Rate constant for photon absorption by LHCs
Km_lightint	115 μE/s m^2	K_m value for light absorption; we assume light saturation at 50 W/m^2 (Geyer and Helms, 2006), i.e. K_m = 25 W/m^2 = 115 μE/s m^2
Exp_lightint	1	
K_RC	746 528 000 mmol gDW^3/h μmol^4	
Km_lh	180 mE/h μmol	K_m value for excitations funneled to RC where charge separation processes takes place (note that maximal turnover rate of RC · LH1 is 1000 Hz)
Exp_lh	1	
K1c	0.26 μmol/gDW	
K1	0.0072 μmol/gDW h	
Km1	1 μmol/gDW	
E1	4	
K2	0.08 μmol/gDW h	
Km2	0.061 %	
E2	4	
Km2Q	1	
E2Q	3	
Km2RC	0.3 μmol/gDW	
E2RC	4	
K3c	1.44	
K3	135 h^{-1}	
Km3	0.43 %	
E3	4	
Km3i	0.15 %	
E3i	4	
K4c	0.449	
K4	36 h^{-1}	
Km4	0.43 %	
Km4i	0.3 %	

Parameter values without references or explanations have been estimated by fitting the measurements given in Table II.

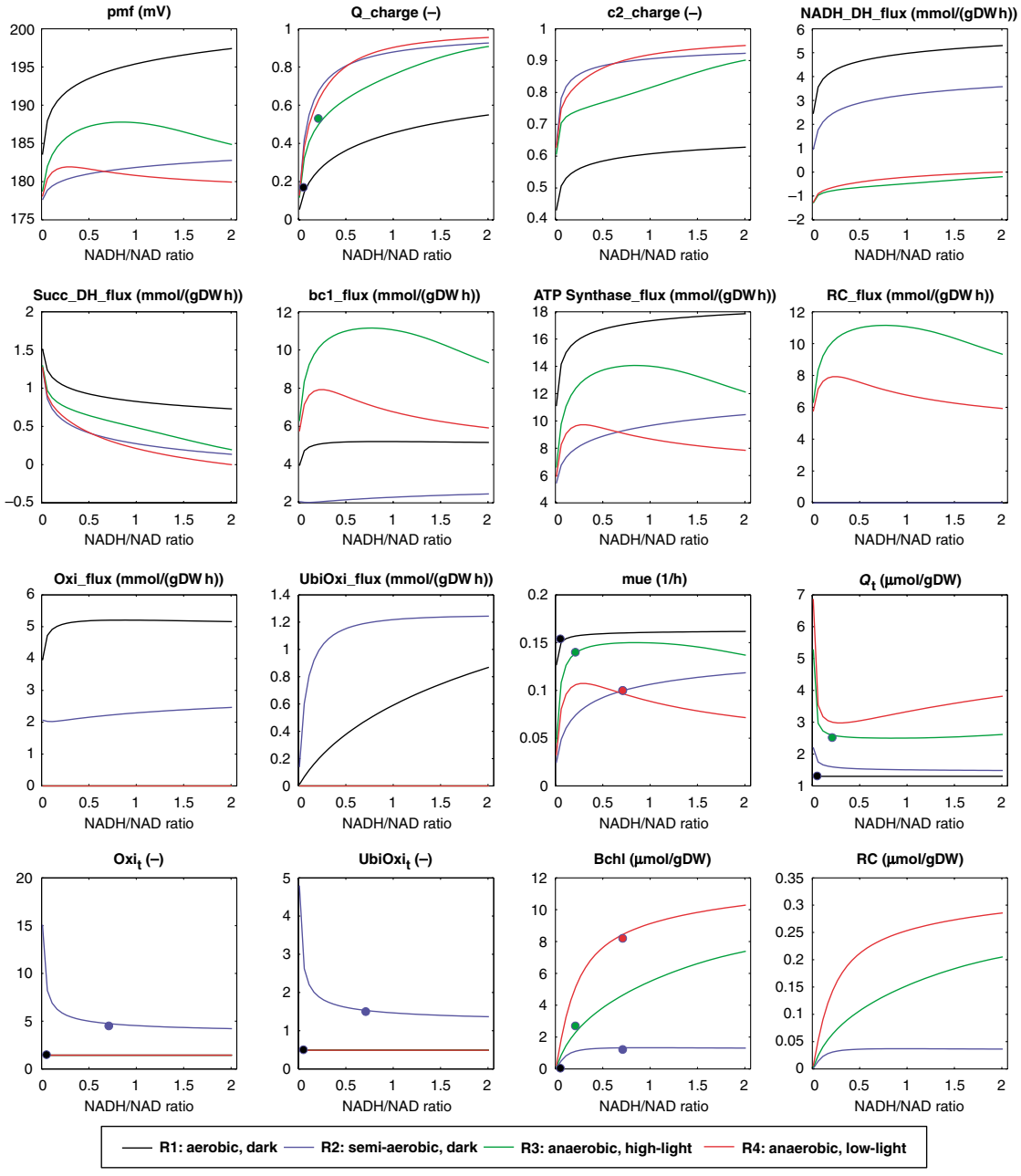

Figure 3 Simulated steady-state response curves of selected model variables for a range of NADH/NAD ratios ($\mathbf{R}_{NADH}$). Four different growth regimens as specified in Table II were considered. Measurements given in Table II are indicated by circles in the respective color. Note that some curves lie on (or very close to) the *x*-axis and partially on top of each other.

model simulations are in a physiologically meaningful range (180–200 mV), even though this has not been taken as a constraint for parameter fitting. This underlines the validity of our model. The model also reproduces correctly that the synthesis of the photosynthetic apparatus and pigments is strongly repressed because neither the oxygen concentration is low nor the ETC is in a reduced state.

Semi-aerobic growth (regimen R2)

The semi-aerobic state is comparably only loosely defined, due to experimental difficulties as well as species-dependent differences. For *R. rubrum*, Grammel *et al* (2003) demonstrated that at oxygen tensions below 0.5%, ICM expression is induced and is accompanied with a specific enzymatic profile.

The simulation of this growth regimen shows that when oxygen becomes limiting, the electron flow to oxygen via the cytochrome oxidase is decelerated. As a consequence, ubiquinone and c_2 are reduced stronger compared to the aerobic case (Figure 3). This effect certainly contributes to higher $\mathbf{R}_{NADH}$ values seen under semi-aerobic conditions (see Table II). The regulatory machinery increases the synthesis of the cbb_3 cytochrome oxidase *and* of the ubiquinol oxidase. Since the

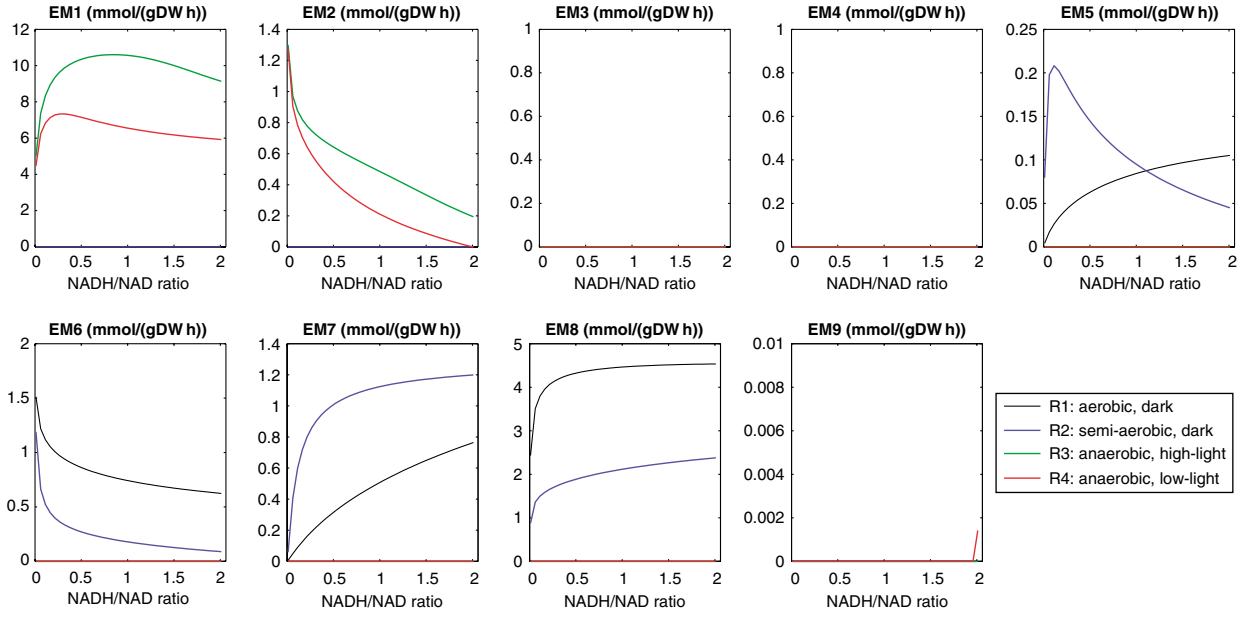

Figure 4 Contribution of the nine elementary modes (Figure 2 and Table I) in the steady-state operation of the kinetic model. As in Figure 3, a response curve for a range of NADH/NAD ratios ($\mathbf{R}_{NADH}$) for the four different growth regimens (Table II) were considered. (For details regarding the computation of these contributions, see Materials and methods.)

electron flow to the final acceptor oxygen now occurs via both oxidases, the elementary modes EM5 and EM7 are now acting concurrently with EM6 and EM8 (Figure 4) thus avoiding an over-reduction of the ETC, though at the expense of lowering the P/O ratio and therefore Δp. With ascending cytosolic redox charge $\mathbf{R}_{NADH}$, the ubiquinol oxidase carries an increasing number of electrons to oxygen because QH_2 becomes available in high amounts. As for regimen R1, reverse electron transport can only be observed when choosing extreme values for $\mathbf{R}_{NADH}$ and/or $\mathbf{R}_{Succ}$. Furthermore, since $\mathbf{R}_{NADH}$ is higher under semi-aerobic conditions, the input of electrons into the ETC occurs now with a higher proportion via the NADH-DH (EM7 and EM8). In contrast, the flux through Succ-DH (EM6) is decreased being in agreement with the fact that the TCA flux in *R. rubrum* is reduced under semi-aerobic and anaerobic conditions (Grammel *et al*, 2003).

In addition, as shown in Figure 3, the induction of ICM synthesis under oxygen-limiting conditions in the dark is correctly reproduced by the model: a considerable amount of BChl and photosynthetic complexes is synthesized, matching the published data.

Anaerobic growth under high light (regimen R3)

When oxygen supply is switched off and light is provided (here with high intensity), a complete reorganization of the composition of the ETC and of the electron flows take place. The repressing signal of oxygen has completely disappeared and photosynthetic membranes and complexes are now synthesized with a higher rate compared to the semi-aerobic case, whereas the expression of oxidases is repressed to a constitutive level. Cyclic photosynthesis (EM1) is now the dominating operational mode in the ETC generating ATP constantly without consumption of electrons. Therefore, electrons fed into the ETC via Succ-DH must leave the ETC again for avoiding over-reduction. In fact, the reaction rate of NADH-DH is now negative and the overall stoichiometry together with the rate of Succ-DH corresponds to the Δp-driven reverse electron transport expressed by EM2 (Figure 4). One might argue that an input of electrons into the ETC and a subsequent energetically expensive reverse flow should be avoided by the cell; however, there are situations where the Succ-DH is necessarily in use, for example, if succinate is the substrate. Note also that a higher reduction level of NADH increases the electron pressure toward the ETC, repressing the reverse flow of electrons from Succ-DH to NADH-DH. For very large $\mathbf{R}_{NADH}$ values (beyond the range considered here), reverse electron flow (EM2) would be replaced by fumarate reduction (EM9).

The reduction degree of ubiquinone and c_2 is significantly larger than in the aerobic regimen R1, even if we would consider the same level for $\mathbf{R}_{NADH}$ (Table II shows that $\mathbf{R}_{NADH}$ tends to be higher under photosynthetic conditions). This is not surprising since oxygen is not available as an electron sink. However, the ETC is less reduced compared to the semi-aerobic regimen (although the validity of this relation strongly depends on which oxygen tension is considered to be 'semi-aerobic'). Growing $\mathbf{R}_{NADH}$ values increase the pressure of electrons into the ETC and the redox state of the ubiquinone (and accordingly the expression of photosynthetic genes) is therefore monotonically dependent on $\mathbf{R}_{NADH}$.

In contrast, another result of our simulations shows that there is a maximum in Δp for photosynthetic conditions: when low $\mathbf{R}_{NADH}$ values are increased, Δp goes up as well because the ETC gets filled with electrons required for driving the photosynthetic cycle. Then, $\mathbf{R}_{NADH}$ reaches an optimum value above which Δp decreases as now the ETC becomes

increasingly over-reduced, impeding the recruitment of Q by the RC. Furthermore, as already mentioned above, Δp under photosynthetic conditions does not reach the high level of the aerobic regimen R1, when identical values for $\mathbf{R}_{NADH}$ are considered in both cases. However, one might choose different $\mathbf{R}_{NADH}$ values (small for R1 and larger for R3, e.g. 0.03 and 0.9, respectively) and a higher Δp would result for photosynthetic growth. Hence, no general statement can be made whether photosynthetic or respiratory growth generates a larger Δp.

Anaerobic growth under low light (regimen R4)

Under low-light conditions, photons become the limiting resource and the overall rate of photosynthesis (see variable *RC_flux* in Figure 3) decreases. The bacteria react upon low light with an increased synthesis of photosynthetic membranes and complexes that, however, can only partially compensate for the reduced photosynthetic flux. The driving force for the amplified expression of the photosynthetic gene cluster can be attributed to the significantly increased reduction degree of ubiquinone. So far, no direct experimental evidence has been given that QH_2/Q_{total} increases when diminishing the light intensity. It is even not clear by intuition: a lowered influx of photons implies that the light-induced transfer of electrons from c_2 to Q is decelerated that could lead to an accumulation of reduced c_2 (which is indeed the case) but not necessarily of QH_2. Our model gives not only a prediction it also gives an explanation for this behavior: due to the lowered photosynthesis rate, the Δp value drops down to about 181 mV. As an implication, the resistance of the ETC against the influx of electrons from NADH via NADH-DH decreases as well (see equation (12) in Materials and methods) leading eventually to a higher reduction degree of ubiquinone. The effect is amplified by the fact that the cytosolic redox state seems to be reduced stronger under low-light conditions.

Importantly, the qualitative behavior of the ubiquinone pool displayed is independent of any model assumption made on the regulation, that is it is a direct effect of the reduced light intensity (and not an indirect effect induced by the activity of regulatory pathways). One might also argue that our result is a matter of the chosen parameter set. Using an evolutionary optimization algorithm (Rechenberg, 1984; Rettinger, 1995), we therefore tried to find a parameter set that brings about the opposite result, that is that the ubiquinone pool is more oxidized under low-light conditions. Even when running the algorithm over days, we could not identify such a parametrization indicating that our findings are indeed a qualitative and structural property of the system.

The fact that the ubiquinone pool gets more reduced under low-light conditions has strong implications: it provides the mechanistic basis for employing the redox state of ubiquinone as an integrated signal for sensing oxygen availability and light intensity that can be used to trigger regulatory events. Our model thus supports the hypothesis that the ubiquinone redox state could be involved in controlling the expression of photosynthetic genes (Oh and Kaplan, 2001; Swem *et al*, 2006). However, one should also be aware of another important aspect when considering the specific amount of BChl and photosynthetic complexes. The growth rate (in our model coupled with the rate of ATP synthesis) usually decreases under limiting low-light conditions implying also a lowered growth-related dilution of photosynthetic components. This may have a profound effect on specific concentrations of photosynthetic components (the latter are not actively degraded): having a cell culture A whose specific content of BChl is twice that of a cell culture B but the growth rate of A is half that of B, then the specific pigment synthesis rate of both cultures is the same. Hence, although the expression rate of photosynthetic genes is certainly increased, a higher specific concentration is partially achieved by the reduced growth rate.

Similar as for high-light conditions, there exists a maximum Δp when increasing $\mathbf{R}_{NADH}$ values, though the optimum occurs at a lower $\mathbf{R}_{NADH}$ level compared to regimen R3 (Figure 3).

A further observation we can make is that for larger $\mathbf{R}_{NADH}$ values (see Figure 4; $\mathbf{R}_{NADH} > 1.95$), the reverse electron transport (EM2) stops and is then replaced by fumarate reduction (EM9), which can be seen for high-light conditions only for even larger $\mathbf{R}_{NADH}$ values.

Model simulations: varying the cellular [ATP]/[ADP] ratio

As we did in the last section for $\mathbf{R}_{NADH}$, we also varied $\mathbf{R}_{ATP}$ in a physiologically meaningful range from 1.5 to 3.5 (and fixed $\mathbf{R}_{NADH}$ and $\mathbf{R}_{Succ}$ to the values given in Table II). As the main result, increasing $\mathbf{R}_{ATP}$ and keeping the two other ratios constant implies a higher Δp for the growth regimens R1–R3: the rate of ATP synthase is decreased because of the high concentration of ATP. As a consequence, the ubiquinone and c_2 pools get more oxidized because the (forward) flows through NADH-DH, bc_1 and the oxidases are reduced as these complexes pump protons against Δp. These effects establish a negative feedback (also known from respiratory control): a high ATP concentration reduces the proton pumping and thus ATP-producing activities in the ETC. Unexpectedly, this behavior appears to be different for photosynthetic growth under low-light conditions (R4): as for the other regimens, Δp increases with $\mathbf{R}_{ATP}$ and ubiquinone and c_2 are less reduced; however, the rate of the cyclic photosynthesis increases as well further contributing to a higher Δp, leading eventually to a higher rate of ATP synthesis. The reason is that larger $\mathbf{R}_{ATP}$ values shift the ETC to a more oxidized state (as reverse electron flow is facilitated by a higher Δp) in which the photosynthetic cycle can be driven more efficiently (remember that the ETC is over-reduced under low-light conditions).

Model simulations: varying the cellular [succinate]/[fumarate] ratio

Finally, we varied $\mathbf{R}_{Succ}$ over two orders of magnitude from 0.1 to 10 and kept $\mathbf{R}_{NADH}$ and $\mathbf{R}_{ATP}$ constant. It turned out that, under all growth regimens, most steady-state values exhibit a remarkable insensitivity against $\mathbf{R}_{Succ}$. This concerns in particular the reduction degrees of ubiquinone and c_2, which remain almost constant over the full range of simulated $\mathbf{R}_{Succ}$. Clearly, a strong change occurs in electron fluxes carried by NADH-DH and Succ-DH, respectively: under aerobic conditions, increasing $\mathbf{R}_{Succ}$ enhances the electron influx into the ETC via Succ-DH (EM5 and EM6 contribute stronger), whereas

the influx of electrons via NADH-DH is thereby lowered (reduced activity for EM7 and EM8). Analogously, under photosynthetic conditions, reverse electron flow takes place with a higher rate due to a higher influx of electrons from succinate.

We also observed that Δp is slightly decreased with growing $\mathbf{R}_{\mathrm{Succ}}$. This can be explained by the fact, that the Succ-DH does not contribute to the generation of Δp (in contrast to NADH-DH whose forward operation is reduced).

Model simulations: aerobic growth in light

We also tested how the model behaves if oxygen and light are available concurrently. The simulation results for this situation should be interpreted with caution because (i) phototoxic effects induced by oxygen radicals, which may occur under these conditions and inhibit growth, are not considered by our model and (ii) modeling the modulation of respiration by light and vice versa might require a compartmentalized model with cytoplasmic and intracytoplasmic membranes. However, we mention here that our model behaves qualitatively correct, that is the synthesis of the photosynthetic apparatus is repressed under high oxygen tension irrespective of the availability of light. Photosynthesis may interfere with respiration only when a photosynthetically grown culture is exposed to oxygen; the repression of the photosynthetic genes will abolish this effect when the photosynthetic units are diluted out. In the steady state, respiration is the dominating operational mode and the ETC behaves virtually as in the aerobic dark case.

Parameter sensitivities and model robustness

As an important step in quantitative modeling, we discuss the robustness of our *in silico* results with respect to parameter uncertainties. As mentioned, several parameters are well defined from literature values (e.g. midpoint redox potentials of ETC components) and the rest has been estimated by fitting the measurements given in Table II. We cannot exclude that other parameter sets fit the measurements also reasonably well. However, albeit we examined *quantitative* (steady state) results from model simulations, most conclusions drawn from the kinetic model are mainly qualitative (e.g. 'ups and downs') and are thus *per se* robust against parameter variations as long as none of the parameters is close to a bifurcation point.

For a rough assessment of the parameter sensitivities, we perturbed each estimated parameter p_j (except exponents in kinetic equations) by a relative level of 10% and analyzed how the model variables x_i (we considered state and algebraic variables) change their steady-state value x_i^{ss}. As a main result, only in about 6% of all cases the model variables changed more than 10% (i.e. only in those cases the approximated relative parameter sensitivities

$$(\partial x_i^{\mathrm{ss}}/x_i^{\mathrm{ss}})/(\partial p_j/p_j)$$

are larger than unity) and thus the model shows a reasonable robustness. Parameters exhibiting larger sensitivities are those involved in the synthesis of ETC components, in particular parameters controlling the synthesis of the photosynthetic apparatus. In addition, several model variables were sensitive with respect to the parameter k_{ATPS}, the rate constant of ATP synthase. This is not surprising since the rate of ATP synthase has a strong effect on Δp which in turn influences the thermodynamic span and thus the rate of several other reactions in the ETC. Finally, as expected, for semi-aerobic growth several variables show a higher sensitivity for the K_{m} values (oxygen saturation) of the two oxidases.

In contrast, very low sensitivities for the *steady states* can be seen for the two parameters describing properties of the membrane compartment, namely *K_leak* (quantifying the strength of proton leak) and *piV* (dependent on buffer capacity and periplasmic volume; see Materials and methods). Most likely, these parameters will have different values for the two membrane types CM and ICM. However, the low sensitivities justify that we have considered identical values for respiratory and photosynthetic growth.

Importantly, the two model variables *Ubi_charge* and *c2_charge,* which reflect the overall redox state of the ETC and which have been discussed intensively in the previous sections, exhibit generally a comparably low sensitivity against parameter variations.

Discussion

In this work, we have presented and analyzed a stoichiometric and kinetic model for the photosynthetic and respiratory operation of the ETC in purple non-sulfur bacteria. Although the stoichiometric model is relatively small (seven reactions) and does not consider any kinetics, it helps to identify the potential functional behaviors of the ETC under photosynthetic, respiratory and fermentative conditions. Apart from the well-known cycles and pathways, the model revealed two operational modes representing reverse electron flow under respiratory conditions. So far, the functional role of reverse electron flow has been mainly discussed for photosynthetic growth only. In fact, due to thermodynamic constraints, reverse electron flow under aerobic conditions plays only a minor role; however, it might become important for certain (possibly temporary) metabolic states, for example, if a great imbalance in the current redox potentials of NADH and succinate occurs. The stoichiometric ETC network model thus demonstrates how stoichiometric modeling helps in identifying—in an unbiased way—meaningful functions of a biochemical network.

Clearly, the stoichiometric model can only show the potential behavior of the ETC. To study the actual driving forces, electron flows and redox states occurring in the ETC under different environmental conditions, we constructed a kinetic model that also includes known regulatory pathways governing the expression of ETC components. To our knowledge, it is the most comprehensive model of the ETC in purple bacteria with respect to the components and processes considered. The reaction steps taking place inside the enzyme complexes have been described with relatively simple, yet thermodynamically justified kinetic laws. We do not claim that our model reproduces ETC states accurately when absolute quantitative units are considered, since available parameters and measurements do not permit this. Nevertheless, it

provides valuable semiquantitative and qualitative insights into the behavior of the ETC, in particular on the redox states of key components that are often difficult to measure. The most important prediction we could derive with our model is that the ubiquinone pool becomes reduced stronger during photosynthetic growth when diminishing the light intensity to a low (limiting) level. Only this behavior qualifies the ubiquinone redox state as a suitable signal for regulating the synthesis of photosynthetic genes as experimental studies have indicated (Oh and Kaplan, 2001; Swem *et al*, 2006).

We mention that light induction of photosynthetic gene expression has also been found to be dependent on photosynthetic electron flow in plant chloroplasts, although the present results about the regulatory role of the redox state of the plastoquinone pool in chloroplast gene expression are conflicting (see for example, Pfannschmidt *et al*, 1999; Matsuo and Obokata, 2002). We think that the modeling approach chosen here is, in principle, extendable by topological constraints for addressing also electron transport phenomena in plant cells, including transfer of reducing equivalents between different energy-converting organelles.

The redox state of ubiquinone is a highly integrative signal. According to our simulations, oxygen availability has the strongest influence, whereas the light intensity, the redox state of cytosolic metabolites exchanging electrons with the ubiquinone pool (such as NADH and succinate) and the ATP concentration do further modulate this signal. The advantage of using an integrated signal for regulation is that the cell requires only one 'measurement device' for sensing different environmental cues. However, combining different signals into one may also lead to some unexpected (for the cell possibly unfavorable) side effects. As we have shown previously for *R. rubrum*, the usage of a special C-substrate combination (fructose and succinate) instead of a standard (succinate) medium, significantly increases the expression of photosynthetic membranes and pigments under semi-aerobic conditions in the dark (Ghosh *et al*, 1994). We have suggested that growth with this substrate combination results in a stronger reduction of the ubiquinone pool, thus interfering with the signaling pathways controlling photosynthetic gene expression (Grammel *et al*, 2003). From our simulations, we can conclude that an increase of $\mathbf{R}_{\mathrm{NADH}}$ and/or a decrease of $\mathbf{R}_{\mathrm{ATP}}$ is most likely responsible for this behavior, whereas the reduction level of ubiquinone is relatively insensitive with respect to $\mathbf{R}_{\mathrm{Succ}}$.

Another interesting result of our model is that for anaerobic photosynthetic growth, there is an optimal value of $\mathbf{R}_{\mathrm{NADH}}$ resulting in the highest possible Δp, and the optimal $\mathbf{R}_{\mathrm{NADH}}$ value depends on the light intensity. Both a too low and a too high reduction degree of NADH limit cyclic photosynthesis because both oxidized and reduced forms of ubiquinone and c_2 are required for driving this cycle. This implies that there is an optimal electron load in the ETC. In contrast, such biphasic phenomena cannot be observed under aerobic conditions: there is a monotone dependency of Δp for arbitrarily high values of $\mathbf{R}_{\mathrm{NADH}}$. Clearly, these considerations assume that the values for $\mathbf{R}_{\mathrm{ATP}}$ and $\mathbf{R}_{\mathrm{Succ}}$ are not directly coupled with $\mathbf{R}_{\mathrm{NADH}}$.

Our kinetic ETC model in its present form provides a mathematical description of the membrane ETC as a first building block, which can be refined or extended in a modular way by additional blocks such as cytoplasmic redox events or a more detailed representation of the mechanisms of redox signaling and redox control of photosynthetic gene expression. The possible refinement of the model by introducing two membrane compartments has already been discussed above.

In the long run, mathematical models, such as the one described in this work, promise to enable a comprehensive theoretical investigation of the redox metabolism of purple bacteria at the systems level.

Materials and methods

Kinetic modeling of electron flows in the ETC

The kinetic ETC model comprises the processes depicted in Figure 1. For the kinetic description of the complicated electron transfer processes, we followed the approach of Korzeniewski (1996a, b) and Korzeniewski and Mazat (1996) by modeling the entirety of elementary steps taking place at an enzyme complex as one (overall) redox reaction. The overall stoichiometries of these reactions correspond to the equations (1–6) and their driving forces are redox potential differences between the two redox couples involved.

The full model with all its (ordinary) differential equations, algebraic relationships and parameters is documented in Table III (model variables) and Table IV (parameters). In the following, we explain some selected equations.

A central variable of the ETC model is the proton-motive force (Δp). The well-known equation for Δp accounts for the electrical gradient (membrane potential $\Delta\Psi$) and the concentration gradient (ΔpH) between the protons in the periplasmic and the cytoplasmic space:

$$\Delta p = \Delta\Psi - 2.303 \cdot R \cdot T \cdot \Delta\mathrm{pH}/F \approx \Delta\Psi - 59\mathrm{mV} \cdot \Delta\mathrm{pH} \qquad (8)$$

(R: gas constant; T=298 K; F=Faraday constant; $\Delta\mathrm{pH}=\mathrm{pH_p}-\mathrm{pH_i}$; $\mathrm{pH_p}$ and $\mathrm{pH_i}$ are the pH values in the periplasmic and cytoplasmic space, respectively). Contrary to ΔpH, the membrane potential $\Delta\Psi$ is not defined by the proton gradient alone, instead it is an integral value that reflects the distribution of all ions at both sides of the membranes. Though only approximately correct (Schuster *et al*, 1998), we follow Korzeniewski (1996a, b) in assuming that there is a linear relationship between ΔpH and $\Delta\Psi$, that is that we can approximate $\Delta\Psi$ from Δp via a constant factor, which could be derived from measurements of Wraight *et al* (1978) and indicates that 30% of the Δp is contributed by ΔpH and 70% by $\Delta\Psi$. We assume additionally that the cytosolic pH is constant ($\mathrm{pH_i}$=7). For bookkeeping the concentration of protons in the periplasmic space, we use a parameter *piV* expressing which amount of $\mathrm{H_i^+}$ (in mmol/gDW) must be pumped over the membrane to increase the concentration of $\mathrm{H_p^+}$ by 1 mM. Clearly, the value of this parameter will strongly depend on many factors such as volume ratios and the buffer capacity of the periplasm, and can only be estimated. However, buffer capacities do not change the steady-state behavior studied herein (but may change the transient behavior). In fact, sensitivity analysis shows that the model results are virtually invariant against varying this parameter over orders of magnitudes. The model considers proton leak also accounting for the escape of protons from the periplasmic space.

As mentioned above, electron transfer processes in complexes such as NADH-DH or bc_1 are modeled as overall redox reactions. The driving force of redox reactions is the redox potential difference ΔE between the two participating redox couples (electron donor (D) and acceptor (A)) which, according to the Nernst equation, can be quantified as

$$\Delta E = \Delta E_{\mathrm{m},7} + \frac{RT}{zF} \cdot \ln \frac{[\mathrm{A^{ox}}][\mathrm{D^{red}}]}{[\mathrm{A^{red}}][\mathrm{D^{ox}}]} \qquad (9)$$

$\Delta E_{\mathrm{m},7}$ (or $\Delta E^{o\prime}$) is the difference in the standard redox (midpoint) potentials of the two redox couples A and D: ($\Delta E_{\mathrm{m},7} = E^{\mathrm{A}}_{\mathrm{m},7} - E^{\mathrm{D}}_{\mathrm{m},7}$) and z is the number of transferred electrons. The redox potential difference is directly coupled with the Gibbs energy change of the redox reaction

$$\Delta G = -z\,F\,\Delta E \qquad (10)$$

In accordance with Korzeniewski (1996a, b) and Korzeniewski and Mazat (1996), we assume that the reaction rate of the redox reaction is proportional to the thermodynamic span (hence proportional to $-\Delta G$) and the amount of available enzyme. Δp and/or $\Delta\Psi$ must be additionally taken into account if protons are pumped and/or electrons are translocated vertically in the membrane. We exemplify the rate equations for the case of the NADH-DH and the bc_1 complex.

NADH-DH transfers two electrons from NADH to Q. For the redox potential difference, we obtain

$$\Delta E_{\mathrm{NADH-DH}} = \Delta E_{\mathrm{m,7}}^{\mathrm{NADH/QH2}} + \frac{RT}{2F}\cdot \ln\frac{[\mathrm{Q}][\mathrm{NADH}]}{[\mathrm{QH_2}][\mathrm{NAD}]} \qquad (11)$$

We know that $\Delta E_{\mathrm{m,7}}^{\mathrm{NADH/QH2}} = 390\,\mathrm{mV}$ since $E_{\mathrm{m,7}}^{\mathrm{Q/QH2}} = +70\,\mathrm{mV}$ and $E_{\mathrm{m,7}}^{\mathrm{NAD/NADH}} = -320\,\mathrm{mV}$. The concentrations of Q and QH_2 are state variables in the model. The ratio [NADH]/[NAD] is fixed prior to simulation (see below). With equation (11) we can quantify the thermodynamic span of the electron transfer from NADH to QH_2; however, we have to consider that the NADH-DH couples the electron transfer by pumping four protons against Δp that reduces the driving force. We thus obtain the following expression for the reaction rate of NADH-DH

$$\begin{aligned} r_{\mathrm{NADH-DH}} &= -k_{\mathrm{NADH-DH}}\Delta G_{\mathrm{NADH-DH}} \\ &= k_{\mathrm{NADH\text{-}DH}} F\,(2\Delta E_{\mathrm{NADH\text{-}DH}} - 4\Delta p) \end{aligned} \qquad (12)$$

which can conveniently be written as

$$r_{\mathrm{NADH\text{-}DH}} = k'_{\mathrm{NADH\text{-}DH}}\,(\Delta E_{\mathrm{NADH\text{-}DH}} - 2\Delta p) \qquad (12')$$

Since $\Delta E_{\mathrm{m,7}}^{\mathrm{NADH/QH_2}}$ is relatively high, the NADH-DH proceeds usually in the forward direction. However, under certain conditions (high levels of Δp and QH_2 and a low level of NADH) the reaction rate may also become negative. This would correspond to the reverse electron flow as discussed in the main text (EM2–EM4 in Table I; Figure 2) where electrons flow from QH_2 to NAD under consumption of Δp.

To evaluate equation (11), the concentration ratio [NADH]/[NAD] is required. Since NADH and NAD are involved in many other metabolic reactions in the cell, it is practically impossible to consider NADH and NAD as state variables in our kinetic model. Therefore, we employ the following strategy: for each of the considered growth regimens—for example, aerobic growth in the dark or anaerobic growth in light—we clamp the ratio of NADH and NAD to a specific value (obtained from measurement data or by reasonable assumptions). The advantage is that we do not need to model the whole cell to get a complete balance for these compounds. However, in the simulations, the assumed (steady state) ratio is immediately fixed for the environmental conditions. For this reason, we focus on the steady-state behavior of the kinetic model. The transient behavior could be interpreted only with caution as, in reality, the levels of NADH and NAD will also be subject to (at least transient) changes after switching, for example, the light or oxygen on or off. We proceeded in the same way with [ATP]/[ADP] and [succinate]/[fumarate].

The rate equation for the bc_1 complex is similar as for NADH-DH:

$$\begin{aligned} r_{bc_1} &= -k_{bc_1}[bc_1]\,\Delta G_{bc_1} \\ &= k_{bc_1}[bc_1]\,F(2\Delta E_{bc_1} - 4(-2.303RT\,\Delta\mathrm{pH}) - 2\Delta\Psi) \end{aligned} \qquad (13)$$

or

$$r_{bc_1} = k'_{bc_1}[bc_1](\Delta E_{bc_1} - 2(-2.303RT\,\Delta\mathrm{pH}) - \Delta\Psi) \qquad (13')$$

There are, however, two differences (i) in contrast to NADH-DH, the concentration of bc_1 is considered explicitly since it is a state variable in the model and subject to regulatory events (see below). (ii) During one Q cycle (eq. (3)), two electrons are transported against the membrane potential (from Q_p (Q_o) to Q_n site of bc_1), whereas four protons are transported against the concentration gradient ΔpH. We note that equation (13) is equivalent to the term

$$r_{bc_1} = k'_{bc_1}[bc_1](\Delta E_{bc_1} - 2\Delta p + \Delta\Psi)$$

used in the mitochondrial models of Korzeniewski (1996a, b) and Beard (2005) since $\Delta p = (-2.303RT\Delta\mathrm{pH} + \Delta\Psi)$.

The rate equation for the Succ-DH is analogous to NADH-DH (eq. (12)), except that the negative term disappears because protons are not pumped over the membrane. The rate equations for the ubiquinol oxidase and cytochrome (cbb_3) oxidase have been modeled analogously to Korzeniewski (1996b) by assuming that the redox state of the *b*-type cytochromes in the oxidases is in near equilibrium with ubiquinone and c_2, respectively (see Table III). Then, electrons flow from these intermediate states to oxygen with Michaelis–Menten kinetics.

For the ATP synthase, we adopt the kinetic approach of Korzeniewski (1996b), which ensures that the rate of ATP synthesis becomes saturated for large Δp values while thermodynamics still being consistent

$$r_{\mathrm{ATPS}} = k_{\mathrm{ATPS}}\frac{e^{\gamma/RT} - 1}{e^{\gamma/RT} + 1} \qquad (14)$$

with

$$\gamma = -\Delta G_{\mathrm{ATPS}} = \Delta G_{0,\,\mathrm{pH=7}}^{\mathrm{ATPHydro}} - RT\,\ln\frac{[\mathrm{ATP}]}{[\mathrm{ADP}]\cdot[P_i]} - 3\cdot\Delta\tilde{\mu}_{\mathrm{H^+}}$$

$\Delta G_{0,\,\mathrm{pH=7}}^{\mathrm{ATPHydro}}$ is the Gibbs energy change of ATP hydrolysis under biological standard conditions (−30.5 kJ/mol) and $\Delta\tilde{\mu}_{\mathrm{H^+}}$ is the proton electrochemical gradient ($\Delta\tilde{\mu}_{\mathrm{H^+}} = -F\Delta p$). The phosphate concentration [P_i] is considered to be constant and the ratio [ATP]/[ADP] is clamped as described for [NADH]/[NAD].

Finally, we need to describe the key reaction steps taking place in the photosynthetic apparatus. The latter consists of LHC and RC (for a detailed description of these complexes, see Nicholls and Ferguson, 2002). There are two types of LHC known as LH1 and LH2. LH1 consists of 32 BChl and 16 carotenoid molecules and surrounds the RC, that is the LH1/RC ratio is 1. LH2 is located further away from the RC (but still close enough to facilitate energy transfer) and consists of 27 BChl and 9 carotenoid molecules. LH1 and LH2 are differently regulated in purple non-sulfur bacteria, thus providing an additional degree of freedom to adapt to varying light conditions (LH2 proportion increases under low-light conditions). As already mentioned, *R. rubrum*—used as model organism herein—does not possess antennae of type LH2. The advantage for modeling is that the total amount *B* of BChl can be directly assigned to LH1 (32/36 *B*) and RC (4/36 *B*). The LHC absorb light energy and transfer it to the RC where the energy is used for charge separation processes.

A detailed description of the processes occurring in the RCs of purple non-sulfur bacteria can be found in Nicholls and Ferguson (2002). Here, we consider a thermodynamic description based on the overall reaction scheme according to equation (6). In this way, the photosynthetic reaction cycle is modeled at the same level of detail as the electron transfer processes described above while retaining thermodynamic consistency. The change in Gibbs energy associated with this reaction scheme is given by

$$\Delta G_{\mathrm{RC}} = -2\mu_\nu - 2F(\Delta E_{\mathrm{RC}} - \Delta\Psi)$$

where we have taken into account that two electrons are transferred against the membrane potential (Nicholls and Ferguson, 2002) and $\mu_\nu = N_{\mathrm{A}}\,h\,\nu\,(1 - T/T_{\mathrm{r}})$ is the Gibbs energy change associated with photon absorption (Meszna and Westerhoff, 1999). Here, N_{A} and h denote Avogadro's and Planck's constant, respectively, while T corresponds to the environmental temperature of the RCs and T_{r} is the temperature of the radiation field, for example, the surface temperature of the sun T_{r}=5000 K. The absorption frequency ν for purple non-sulfur bacteria corresponds to a wavelength of approximately 870 nm. For the reaction rate of the photosynthetic cycle, we use an adaption of the expression given in Meszna and Westerhoff (1999)

$$r_{\mathrm{RC}} = k_{\mathrm{RC}}\,I\,(e^{\alpha}[\mathrm{Q}]\,[c_2^{2+}]^2 - [\mathrm{QH_2}][c_2^{3+}]^2) \qquad (15)$$

with $\alpha = \frac{2F}{RT}(\Delta E_{\mathrm{m,7}}^{\mathrm{Q/QH_2}} - \Delta E_{\mathrm{m,7}}^{c2(3+)/c2(2+)} + \frac{N_{\mathrm{A}}h\nu}{F}\cdot(1 - T/T_{\mathrm{r}}) - \Delta\Psi)$ and where I depends on the number of photons collected (which in turn depends on the number of LHCs) and on the number of RCs (for a detailed expression, see Table III). Equation (15) may be rewritten as

$$r_{\mathrm{RC}} = k'_{\mathrm{RC}}I(e^{-2F\Delta\Psi/(RT)}[\mathrm{Q}][c_2^{2+}]^2 - e^{-\beta}[\mathrm{QH_2}][c_2^{3+}]^2) \qquad (15')$$

with

$$\beta = \frac{2F}{RT}(\Delta E_{m,7}^{Q/QH_2} - \Delta E_{m,7}^{c2(3+)/c2(2+)} + \frac{N_A h\nu}{F} \cdot (1 - T/T_r)) \approx \frac{2F}{RT}(\Delta E_{m,7}^{Q/QH_2} - \Delta E_{m,7}^{c2(3+)/c2(2+)} + 1340\,\text{mV})$$

Modeling regulatory pathways

The composition of the ETC and the formation of photosynthetic membranes in purple bacteria are mainly governed by the external signals oxygen and, to a lower extent, light intensity and the supply of reducing equivalents by the carbon substrate (Oh and Kaplan, 2001; Bauer, 2004). Although our model focuses on the operation of the ETC, we need to include basic regulatory events such that the photosynthetic apparatus consisting of LHC and RC is synthesized under anaerobic conditions. The molecular basis of the regulation of the photosynthetic gene cluster containing the genes for BChl (*bch*) and carotenoid (*crt*) biosynthesis, and for LHC polypeptides (*puc* and *puf*) and the RC subunits (*puh* and *puf*) (Alberti *et al*, 1995), has been studied in detail in *Rb. capsulatus* and *Rb. sphaeroides* (Oh and Kaplan, 2001; Bauer, 2004) and appears to be conserved, including in *R. rubrum* (Addlesee and Hunter, 2002). Three major regulators have been identified that control the expression of genes in the PGC and those involved in the synthesis of other ETC components such as ubiquinone, c_2 as well as of the ubiquinol and the cytochrome (cbb_3) oxidase

(i) The RegB/RegA (PrrB/PrrA) two-component system with the global regulator RegA activates the expression of genes involved in respiration (e.g. oxidases), photosynthesis (PGC), CO2 fixation, nitrogen fixation and hydrogen release (Swem *et al*, 2001; Elsen *et al*, 2004). It is still under debate what the initial signal for autophosphorylation of RegB is. The cbb_3 oxidase has been demonstrated to generate an inhibiting signal for RegB autophosphorylation (Oh and Kaplan, 2000). Recent works indicate that RegB activity is triggered by the redox state of the ubiquinone pool (Swem *et al*, 2006), similar to the mechanism of the global ArcB sensor kinase in *Escherichia coli* (Georgellis *et al*, 2001). Under reducing conditions, the RegB autophosphorylates and subsequently phosphorylates and thereby activates the transcription activator RegA.

(ii) Another regulator is FnrL (Fnr-like protein), a homolog of the global regulator Fnr known in many other bacteria, including *E. coli*. Under anaerobic conditions, with an unknown mechanism, FnrL dimerizes to its active form and enhances, among others, the expression of cytochrome c_2, cbb_3 and some photosynthetic genes including those required for LH2 formation (Zeilstra-Ryalls *et al*, 1997; Zeilstra-Ryalls and Kaplan, 1998; Oh and Kaplan, 2001).

(iii) A repressor of photosynthetic genes is PpsR (CrtJ). Under aerobic conditions, PpsR binds to its target promotors in the PGC, thereby blocking their expression (Elsen *et al*, 2005; Kovacs *et al*, 2005). Regarding the triggered signal, it was considered that PpsR might have the capability of sensing redox changes through the formation of disulfide bond(s) (Masuda and Bauer, 2002), but it remains still unknown what the actual input signal is. PpsR signaling becomes more complicated by the fact that AppA (known in *Rb. capsulatus*, not in *Rb. sphaeroides*) behaves as an antirepressor of PpsR. AppA itself is influenced by redox signals and may reduce its antirepressor activity when exposed to blue light (Masuda and Bauer, 2002).

In the differential equations for LHC, RC and other ETC components, we included kinetic terms expressing the dependency of the synthesis of the ETC components on the oxygen tension and the redox state of the ubiquinone pool mimicking the combined effects of the regulators AppA/PpsR, FnrL and RegB/RegA (compare with Table III):

- Expression of LHC and RC depends negatively on oxygen and positively on the reduction degree of ubiquinone. Note that the latter is rather a hypothesis than an ascertained fact and our model aims at verifying whether the reduction degree of ubiquinone is a suitable signal for regulating LHC and RC expression or not (i.e. whether we can reproduce the macroscopic behavior of LHC/RC synthesis).
- Since we focus here on *R. rubrum*, LH2 is not considered and the ratio of LH1/RC is constant.
- For the expression of c_2, we included a repressive effect of oxygen (Oh and Kaplan, 2001). For ubiquinone and bc_1, we assume a constant ratio (25 and 0.6) of their total concentrations to c_2 (cf. measurements given by Garcia *et al*, 1987).
- For the two oxidases, we assumed a positive (via FnrL) as well as a repressive effect of oxygen (via RegA (PrrA), see Eraso and Kaplan, 2002), thus ensuring the highest synthesis of oxidases under semi-aerobic conditions and basal levels for aerobic and anaerobic growth (Swem and Bauer, 2002).
- We hold the concentrations for NADH-DH and Succ-DH constant for all conditions since only little data concerning their regulation is available.

We did not include a direct regulatory effect of light (intensity). One reason is that (except for the aforementioned blue light inactivation of AppA exclusively shown in *Rb. capsulatus*) none of the three major regulators is under direct control of light.

Decomposing the fluxes in the ETC into EMs

Having the kinetic model simulated, we can use the calculated steady-state flux values in the ETC to determine the relative contribution of the elementary modes (Table I and Figures 2 and 4) for the simulated scenario. A reaction flux vector in a stoichiometric network can always be decomposed into a weighted sum of EMs but this decomposition is usually not unique and several different decomposition algorithms have been proposed (Schwartz and Kanehisa, 2006). However, in the case of the nine EMs computed for the ETC, with the following reasonable assumptions the decomposition of a given flux vector is straightforward:

- As in the dynamic simulations, we do not consider combined activity of photosynthesis and respiration.
- If ubiquinol oxidase (*UbiOxi_flux* >0) and cytochrome oxidase (*Oxi_flux* >0) operate concurrently, we assume that their relative contributions in respiration with succinate (EM5 and EM6) and with NADH (EM7 and EM8) as electron donor as well as in aerobic reverse electron flow (EM3 and EM4) are distributed as the ratio of these two fluxes.
- EMs are arbitrarily scaleable. Here, we assume EM1 to be normalized on *RC_flux*, EM2, EM5, EM6 and EM9 on *Succ_DH_flux* and EM3, EM4, EM7 and EM8 on *NADH_DH_flux* and then compute the respective coefficients.
- Proton leak (considered in the dynamic model but not explicitly in the stoichiometric model) is subsumed as equivalent proton efflux in the ATP synthase flux.

With these assumptions, for a given steady-state flux vector of the dynamic model we can assign the relative activity for each EM with the following simple rules (for variable names, see Table III):

```
EM1 = EM2 = EM3 = EM4 = EM5 = EM6 = EM7 = EM8 = EM9 = 0;
if(Succ_DH_flux < 0)  %% Fumarate Reduction
   EM9 = -Succ_DH_flux;
end
respflux = Oxidase_flux + UbiOxidase_flux;
if(respflux = = 0)
   if(RC_s1s2_flux > 0)  %% photosynthesis
      EM1 = RC_flux;
      if(Succ_DH_flux > 0)    %% photosynthetic reverse electron flow
         EM2 = Succ_DH_flux;
         EM1 = EM1-Succ_DH_flux;  %% subtract photosynthesis flux
for reverse electron flow
      end
   end
else %% Respiration
   if(NADH_DH_flux < 0)       %% aerobic reverse electron flow
      EM3 = -UbiOxidase_flux*NADH_DH_flux/respflux;
      EM4 = -Oxidase_flux*NADH_DH_flux/respflux;
   elseif(NADH_DH_flux > 0)     %% respiration with NADH
      EM7 = UbiOxidase_flux*(NADH_DH_flux-EM9)/respflux;
      EM8 = Oxidase_flux*(NADH_DH_flux-EM9)/respflux;
   end
   if(Succ_DH_flux > 0)    % respiration with electron from succinate
      EM5 = UbiOxidase_flux*(Succ_DH_flux-EM3)/respflux;
      EM6 = Oxidase_flux*(Succ_DH_flux-EM4)/respflux;
   end
end
```

Model implementation and availability

The full model comprises 33 time-dependent variables of which 10 are states (mathematically expressed by differential equations); the rest depends algebraically upon the state variables (Table III). The model has 55 parameters; 17 of them could be directly taken (or estimated) from literature values. The other 38 parameters were estimated by fitting an available set of measurements given in Table II.

We implemented and simulated the ETC model with self-written MATLAB scripts and implemented it additionally with the Systems Biology Toolbox (Schmidt and Jirstrand, 2006; http://www.sbtoolbox.org/) for MATLAB. The input file for the Systems Biology Toolbox can be downloaded from http://www.mpi-magdeburg.mpg.de/projects/cna/etcmodel.html.

Supplementary information

Supplementary information is available at the *Molecular Systems Biology* website (www.nature.com/msb).

Acknowledgements

We thank Michael Ederer and Stefan Schuster for stimulating discussions and valuable comments. We are also grateful to the German Federal Ministry of Education and Research (FORSYS) and the Ministry of Education of Saxony-Anhalt (Research Center 'Dynamic Systems') for support.

References

Addlesee HA, Hunter CN (2002) *Rhodospirillum rubrum* possesses a variant of the bchP gene, encoding geranylgeranyl-bacteriopheophytin reductase. *J Bacteriol* **184:** 1578–1586

Alberti M, Burke DH, Hearst JE (1995) Structure and sequence of the photosynthesis gene cluster. In *Anoxygenic Photosynthetic Bacteria*, Blankenship RE, Madigan MT, Bauer CE (eds) pp 1083–1106. Dordrecht: Kluwer Academic Publishers

Bauer C (2004) Regulation of photosystem synthesis in *Rhodobacter capsulatus*. *Photosynth Res* **80:** 353–360

Bauer C, Elsen S, Swem LR, Swem D, Masuda S (2003) Redox and light regulation of gene expression in photosynthetic prokaryotes. *Philos Trans R Soc Lond B Biol Sci* **358:** 147–154

Beard DA (2005) A biophysical model of the mitochondrial respiratory system and oxidative phosphorylation. *PLoS Comput Biol* **1:** e36

Berry S, Rumberg B (2000) Kinetic modeling of the photosynthetic electron transport chain. *Bioelectrochemistry* **53:** 35–53

Carr GN, Exell G (1965) Ubiquinone concentrations in *Arthiorhodaceae* grown under various experimental conditions. *Biochem J* **96:** 688–692

Cohen-Bazire G, Sistrom WR, Stanier RY (1957) Kinetic studies of pigment synthesis by non-sulfur purple bacteria. *J Cell Comp Physiol* **49:** 25–68

Deisenhofer J, Epp O, Miki K, Huber R, Michel H (1985) Structure of the protein subunits in the photosynthetic reaction centre of *Rhodopseudomonas viridis* at 3 Å resolution. *Nature* **318:** 618–624

Drews G, Golecki JR (1995) Structure, molecular organization, and biosynthesis of membranes of purple bacteria. In *Anoxygenic Photosynthetic Bacteria*, Blankenship RE, Madigan MT, Bauer CE (eds) pp 231–257. Dordrecht: Kluwer Academic Publishers

Elsen S, Jaubert M, Pignol D, Giraud E (2005) PpsR: a multifaceted regulator of photosynthesis gene expression in purple bacteria. *Mol Microbiol* **57:** 17–26

Elsen S, Swem LR, Swem DL, Bauer CE (2004) RegB/RegA, a highly conserved redox-responding global two-component regulatory system. *Microbiol Mol Biol Rev* **68:** 263–279

Eraso JM, Kaplan S (2002) Redox flow as an instrument of gene regulation. *Methods Enzymol* **348:** 216–229

ETC model files (2000) http://www.mpi-magdeburg.mpg.de/projects/cna/etcmodel.html

Garcia AF, Venturoli G, Gad'on N, Fernandez-Velasco JG, Melandri BA, Drews G (1987) The adaption of the electron transfer chain of *Rhodopseudomonas capsulata* to different light intensities. *Biochim Biophys Acta* **890:** 335–345

Georgellis D, Kwon O, Lin EC (2001) Quinones as the redox signal for the arc two-component system of bacteria. *Science* **292:** 2314–2316

Geyer T, Helms V (2006) Reconstruction of a kinetic model of the chromatophore vesicles from *Rhodobacter sphaeroides*. *Biophys J* **91:** 927–937

Geyer T, Lauck F, Helms V (2007) Molecular stochastic simulations of chromatophore vesicles from *Rhodobacter sphaeroides*. *J Biotechnol* **129:** 212–228

Ghosh R, Hardmeyer A, Thoenen I, Bachofen R (1994) Optimization of the sistrom medium for large-scale batch cultivation of *Rhodospirillum rubrum* under semiaerobic conditions with maximal yield of photosynthetic membranes. *Appl Environ Microbiol* **60:** 1698–1700

Grammel H, Gilles ED, Ghosh R (2003) Microaerophilic cooperation of reductive and oxidative pathways allows maximal photosynthetic membrane biosynthesis in *Rhodospirillum rubrum*. *Appl Environ Microbiol* **69:** 6577–6586

Holt SC, Marr AG (1965) Effect of light intensity on the formation of intracytoplasmatic membrane in *Rhodospirillum rubrum*. *J Bacteriol* **89:** 1421–1429

Imhoff JF, Bias-Imhoff U (1995) Lipids, quinones and fatty acids of anoxygenic phototrophic bacteria. In *Anoxygenic Photosynthetic Bacteria*, Blankenship RE, Madigan MT, Bauer CE (eds) pp 179–205. Dordrecht: Kluwer Academic Publishers

Karrasch S, Bullough PA, Ghosh R (1995) The 8.5 Å projection map of the light-harvesting complex I from *Rhodospirillum rubrum* reveals a ring composed of 16 subunits. *EMBO J* **18:** 534–542

Klamt S, Saez-Rodriguez J, Gilles ED (2007) Structural and functional analysis of cellular networks with CellNetAnalyzer. *BMC Syst Biol* **1:** 2

Klamt S, Schuster S, Gilles ED (2002) Calculability analysis in underdetermined metabolic networks illustrated by a model of the central metabolism in purple nonsulfur bacteria. *Biotechnol Bioeng* **77:** 734–751

Klamt S, Stelling J (2006) Stoichiometric and constraint-based modeling. In *System Modeling in Cellular Biology: from Concepts to Nuts and Bolts*, Szallasi Z, Stelling J, Periwal V (eds) pp 73–96. Cambridge: MIT Press

Korzeniewski B (1996a) Simulation of state 4→state 3 transition in isolated mitochondria. *Biophys Chem* **57:** 143–153

Korzeniewski B (1996b) Simulation of oxidative phosphorylation in hepatocytes. *Biochem Chem* **58:** 215–224

Korzeniewski B, Mazat JP (1996) Theoretical studies on the control of oxidative phosphorylation in muscle mitochondria: application to mitochondrial deficiencies. *Biochem J* **319:** 142–148

Kovacs AT, Rakhely G, Kovacs KL (2005) The PpsR regulator family. *Res Microbiol* **156:** 619–625

Masuda S, Bauer CE (2002) AppA is a blue light photoreceptor that antirepresses photosynthesis gene expression in *Rhodobacter sphaeroides*. *Cell* **110:** 613–623

Matsuo M, Obokata J (2002) Dual roles of photosynthetic electron transport in photosystem I biogenesis: light induction of mRNAs and chromatic regulation at post-mRNA level. *Plant Cell Physiol* **43:** 1189–1197

McDermott G, Prince SM, Freer AA, Hawthornthwaite-Lawless AM, Papiz MZ, Cogdell RJ, Isaacs NW (1995) Crystal structure of an integral membrane light-harvesting complex from photosynthetic bacteria. *Nature* **374:** 517–521

Meszna G, Westerhoff HV (1999) Non-equilibrium thermodynamics of light absorption. *J Phys A Math Gen* **32:** 301–311

Microbial Genomics (2000) http://genome.jgi-psf.org/mic_home.html

Nicholls DG, Ferguson SJ (2002) *Bioenergetics 3*. London, UK: Academic Press

Oh J, Kaplan S (2000) Redox signaling: globalization of gene expression. *EMBO J* **19:** 4237–4247

Oh J, Kaplan S (2001) Generalized approach to the regulation and integration of gene expression. *Mol Microbiol* **39:** 1116–1123

Pfannschmidt T, Nilsson A, Allen JF (1999) Photosynthetic control of chloroplast gene expression. *Nature* **397:** 625–628

Price ND, Reed JL, Palsson BO (2004) Genome-scale models of microbial cells: evaluating the consequences of constraints. *Nat Rev Microbiol* **2:** 886–897

Rechenberg I (1984) The evolutionary strategy—a mathematical model of Darwinian evolution. In *Synergetics—from Microscope to Macroscopic Order*, Frehland E (ed) pp 122–132. Berlin-Heidelberg: Springer

Redfarn ER (1967) Redox reactions of ubiquinone in *Rhodospirillum rubrum*. *Biochim Biophys Acta* **131:** 218–220

Rettinger A (1995) Parameteroptimierung mittels Evolutionsstrategien. Studienarbeit, Institut für Systemdynamik und Regelungstechnik, University of Stuttgart

Schmidt H, Jirstrand M (2006) Systems Biology Toolbox for MATLAB: a computational platform for research in systems biology. *Bioinformatics* **15:** 514–515

Schön G (1969) Der Einfluß der Kulturbedingungen auf den ATP-, ADP- und AMP-Spiegel bei *Rhodospirillum rubrum*. *Arch Mikrobiol* **66:** 348–364

Schön G (1971) Der Einfluß der Kulturbedingungen auf den Nicotin-Adenin-Dinucleotid(phosphat)-Gehalt in Zellen von *Rhodospirillum rubrum*. *Arch Mikrobiol* **68:** 147–163

Schuster S, Fell D, Dandekar T (2000) A general definition of metabolic pathways useful for systematic organization and analysis of complex metabolic networks. *Nat Biotechnol* **18:** 326–332

Schuster S, Ouhabi R, Rigoulet M, Mazat JP (1998) Modelling the interrelation between the transmembrane potential and pH difference across membranes with electrogenic proton transport upon build-up of proton-motive force. *Bioelectrochem Bioenerg* **45:** 181–192

Schwartz JM, Kanehisa M (2006) Quantitative elementary mode analysis of metabolic pathways: the example of yeast glycolysis. *BMC Bioinformatics* **7:** 186

Swem DL, Bauer CE (2002) Coordination of ubiquinol oxidase und cytochrome cbb_3 oxidase expression by multiple regulators in *Rhodobacter capsulatus*. *J Bacteriol* **184:** 2815–2820

Swem LR, Elsen S, Bird TH, Swem DL, Koch HG, Myllykallio H, Daldal F, Bauer CE (2001) The RegB/RegA two-component regulatory system controls synthesis of photosynthesis and respiratory electron transfer components in *Rhodobacter capsulatus*. *J Mol Biol* **309:** 121–138

Swem LR, Gong X, Yu CA, Bauer CE (2006) Identification of a ubiquinone-binding site that affects autophosphorylation of the sensor kinase RegB. *J Biol Chem* **81:** 6768–6775

Systems Biology Toolbox (2000) http//www.sbtoolbox.org/

Tabita FR (1995) The biochemistry and metabolic regulation of carbon metabolism and CO_2-fixation in purple bacteria. In *Anoxygenic Photosynthetic Bacteria*, Blankenship RE, Madigan MT, Bauer CE (eds) pp 885–914. Dordrecht: Kluwer Academic Publishers

Trumpower BL (1990) The protonmotive Q cycle. *J Biol Chem* **265:** 11409–11412

Varela J, Ramirez JM (1990) Oxygen-linked electron transfer and energy conservation in *Rhodospirillum rubrum*. In *Anoxygenic Photosynthetic Bacteria*, Blankenship RE, Madigan MT, Bauer CE (eds) pp 443–452. Dordrecht: Kluwer Academic Publishers

Vermeglio A, Joliot P, Joliot A (1995) Organization of electron transfer components and supercomplexes. In *Anoxygenic Photosynthetic Bacteria*, Blankenship RE, Madigan MT, Bauer CE (eds) pp 279–295. Dordrecht: Kluwer Academic Publishers

Wraight CA, Cogdell RJ, Chance B (1978) Ion transport and electrochemical gradients in photosynthetic bacteria. In *The Photosynthetic Bacteria*, Clayton RK, Sistrom WR (eds) pp 471–511. New York: Plenum Press

Zannoni D (1995) Aerobic and anaerobic electron transport chains in anoxygenic phototrophic bacteria. In *Anoxygenic Photosynthetic Bacteria*, Blankenship RE, Madigan MT, Bauer CE (eds) pp 949–971. Dordrecht: Kluwer Academic Publishers

Zeilstra-Ryalls JH, Gabbert K, Mouncey NJ, Kaplan S, Kranz RG (1997) Analysis of the *fnrL* gene and its function in *Rhodobacter capsulatus*. *J Bacteriol* **179:** 7264–7273

Zeilstra-Ryalls JH, Kaplan S (1998) Role of the fnrL gene in photosystem gene expression and photosynthetic growth of *Rhodobacter sphaeroides* 2.4.1. *J Bacteriol* **180:** 1496–1503